

Learning from B Cell Evolution: Adaptive Multi-Expert Diffusion for Antibody Design via Online Optimization

Hanqi Feng^{1*}, Peng Qiu^{1*}, Mengchun Zhang^{2*}, Yiran Tao¹, You Fan³, Jingtao Xu⁴, Barnabas Poczos^{1†}

¹School of Computer Science, Carnegie Mellon University

²Department of Biostatistics, University of Pittsburgh

³Department of Mathematics, King’s College London

⁴Department of Statistics, London School of Economics and Political Science
{hanqif, pengq, bpoczso}@cs.cmu.edu, andy0814xu@gmail.com

Abstract

Recent advances in diffusion models have shown remarkable potential for antibody design, yet existing approaches apply uniform generation strategies that cannot adapt to each antigen’s unique requirements. Inspired by B cell affinity maturation—where antibodies evolve through multi-objective optimization balancing affinity, stability, and self-avoidance—we propose the first biologically-motivated framework that leverages physics-based domain knowledge within an online meta-learning system. Our method employs multiple specialized experts (van der Waals, molecular recognition, energy balance, and interface geometry) whose parameters evolve during generation based on iterative feedback, mimicking natural antibody refinement cycles. Instead of fixed protocols, this adaptive guidance discovers personalized optimization strategies for each target. Our experiments demonstrate that this approach: (1) discovers optimal SE(3)-equivariant guidance strategies for different antigen classes without pre-training, preserving molecular symmetries throughout optimization; (2) significantly enhances hotspot coverage and interface quality through target-specific adaptation, achieving balanced multi-objective optimization characteristic of therapeutic antibodies; (3) establishes a paradigm for iterative refinement where each antibody-antigen system learns its unique optimization profile through online evaluation; (4) generalizes effectively across diverse design challenges, from small epitopes to large protein interfaces, enabling precision-focused campaigns for individual targets.

Introduction

Computational antibody design remains a fundamental challenge in therapeutic development, requiring simultaneous optimization of hotspot coverage, structural stability, and binding interface quality (Fischman and Ofra 2018; Norman et al. 2020). While recent diffusion-based methods like RFdiffusion (Watson et al. 2023) and RFAntibody (Luo et al. 2022) show promise for generating novel protein structures, they lack mechanisms to incorporate real-time constraints during generation, often producing designs that fail to meet multiple competing objectives (Eguchi et al. 2022).

Current approaches face three fundamental limitations: (1) they generate structures through diffusion without target-

specific guidance (Watson et al. 2023; Trippe et al. 2023), (2) they cannot balance multiple objectives during generation, requiring inefficient post-hoc filtering (Jin et al. 2022; Shuai, Ruffolo, and Gray 2021), and (3) they either ignore physical constraints or require extensive labeled data to train property predictors (Dauparas et al. 2022; Hsu et al. 2022). These limitations significantly reduce their effectiveness for therapeutic antibody design, where each target presents unique challenges (Akbar et al. 2022; Mason et al. 2021).

We present an adaptive guidance framework that addresses these limitations by introducing physics-aware constraints directly into the SE(3)-equivariant diffusion process (Hooeboom et al. 2022; Corso et al. 2023). Our contributions include:

- **Multi-expert guidance system:** We develop specialized guidance modules for van der Waals interactions (Jumper et al. 2021), molecular recognition (Gainza et al. 2020), energy balance (Ingraham et al. 2019), and interface geometry (Schneider et al. 2022), each providing targeted gradients during diffusion while maintaining equivariance (Satorras, Hooeboom, and Welling 2021a).
- **Novel expert routing:** A dynamic routing system activates appropriate experts based on real-time structural metrics and diffusion timestep, ensuring optimal constraint application throughout generation (Xue et al. 2015; Olympiou et al. 2022).
- **Online parameter adaptation:** Using Bayesian optimization with Gaussian processes, our framework learns optimal guidance strategies for each antigen-antibody pair through iterative batch evaluation, automatically discovering target-specific temporal profiles without requiring pre-training (Raybould et al. 2019; Shanehsazadeh et al. 2023).

Experiments across diverse targets demonstrate substantial improvements: 7% reduction in CDR-H3 RMSD, 9% increase in hotspot coverage, 12% better interface pAE, and 5% higher shape complementarity, with enhanced metrics across all evaluation criteria. This balanced optimization addresses the critical “weakest link” problem (Raybould et al. 2019) in antibody design. By combining physics-based guidance with online learning, our work opens new directions for adaptive approaches in biomolecular design.

*These authors contributed equally.

†Corresponding author

Related Work

Computational Antibody Design

The field has evolved from physics-based approaches using Rosetta (Kaufmann et al. 2010) and MODELLER (Webb and Sali 2016) to deep learning methods inspired by AlphaFold2 (Jumper et al. 2021). DeepAb (Ruffolo, Sulam, and Gray 2022) pioneered deep learning for antibody structure prediction, while ABlooper (Abanades et al. 2022) focused on CDR-H3 modeling.

Recent generative approaches shifted to de novo design. DiffAb (Luo et al. 2022) introduced diffusion models for joint sequence-structure generation but operates in internal coordinates, limiting inter-chain modeling. RFAntibody (Adolf-Bryfogle, Toth, and Bahl 2024) addressed this using SE(3)-equivariant backbone generation in Cartesian space. However, current methods lack both physicochemical constraint enforcement and target-specific adaptation during generation. This results in high-throughput campaigns producing substantial fractions of structurally unreasonable or experimentally nonviable designs (Shen et al. 2024). Additional related work is discussed in Appendix A due to space limitations.

Preliminaries

SE(3)-Equivariant Diffusion Models

Protein structure modeling requires respecting 3D spatial symmetries. RFdiffusion (Watson et al. 2023) combines SE(3)-equivariant networks with diffusion models, performing diffusion directly on backbone coordinates while maintaining rotational and translational equivariance.

Frame Representations and Forward Diffusion Process

Each residue i is represented by a rigid body frame $\mathbf{T}_i = (\mathbf{R}_i, \mathbf{t}_i) \in \text{SE}(3)$, where $\mathbf{R}_i \in \text{SO}(3)$ is a rotation matrix and $\mathbf{t}_i \in \mathbb{R}^3$ is a translation vector. For N residues, the complete structure is $\mathbf{T} = \{\mathbf{T}_1, \dots, \mathbf{T}_N\}$.

The forward diffusion process adds noise over time steps $t \in \{0, 1, \dots, T\}$. Rotations follow the IGSO3 distribution, $q(\mathbf{R}_t | \mathbf{R}_0) = \text{IGSO3}(\mathbf{R}_t; \mathbf{R}_0, \sigma_t)$ with density:

$$f(\mathbf{R}_t | \mathbf{R}_0, \sigma_t) = \frac{1}{Z(\sigma_t)} \exp\left(-\frac{\text{tr}(\mathbf{R}_0^T \mathbf{R}_t)}{\sigma_t^2}\right) \quad (1)$$

where σ_t is the noise level at timestep t , controlling the variance of the distribution (Yim et al. 2023). The derivation of the score function and its properties on the $\text{SO}(3)$ manifold are detailed in Appendix B. Translations follow Gaussian diffusion with center-of-mass constraint:

$$q(\mathbf{t}_t | \mathbf{t}_0) = \mathcal{N}(\mathbf{t}_t; \mathbf{t}_0, \sigma_t^2 \mathbf{I}_3), \quad \text{s.t.} \quad \sum_{i=1}^N \mathbf{t}_{t,i} = \sum_{i=1}^N \mathbf{t}_{0,i} \quad (2)$$

Reverse Diffusion and Network Architecture The reverse process learns to denoise the forward diffusion process by estimating clean structure \mathbf{T}_0 from noisy \mathbf{T}_t (Ho, Jain, and Abbeel 2020):

$$p_\theta(\mathbf{T}_{t-1} | \mathbf{T}_t) = p(\mathbf{T}_{t-1} | \mathbf{T}_t, \hat{\mathbf{T}}_0), \quad (3)$$

$$\hat{\mathbf{T}}_0 = \frac{1}{\sqrt{\bar{\alpha}_t}} (\mathbf{T}_t - \sqrt{1 - \bar{\alpha}_t} \epsilon_\theta(\mathbf{T}_t, t)) \quad (4)$$

where $\bar{\alpha}_t = \prod_{s=1}^t \alpha_s$ is the cumulative product of noise schedule parameters, and $\epsilon_\theta(\mathbf{T}_t, t)$ is the neural network with parameters θ that predicts the noise added at timestep t .

RFAntibody Pipeline

RFAntibody (Adolf-Bryfogle et al. 2024) employs a three-stage pipeline for antibody design: (1) RFdiffusion generates diverse antibody backbones conditioned on the target antigen, (2) ProteinMPNN designs sequences compatible with these structures, and (3) RoseTTAFold2 validates the designs by predicting their folded structures. This decoupled approach allows each model to focus on its specialized task—structure generation, sequence design, and validation respectively. The pipeline filters designs based on structural quality metrics, retaining only those most likely to succeed experimentally.

Problem Formulation and Motivation

While state-of-the-art generative models excels at generating diverse protein structures, it faces a critical challenge in antibody design: maintaining balanced performance across multiple essential metrics. In antibody engineering, success requires simultaneous optimization of structural accuracy (CDR-H3 RMSD), prediction confidence (pAE, ipAE), interface quality (shape complementarity, buried surface area), and biophysical properties (VDW interactions, stability) (Raybould et al. 2019; Norman et al. 2020; Choi et al. 2018).

The fundamental issue is that RFdiffusion’s purely data-driven approach lacks mechanisms to enforce multi-objective balance. This leads to the “weakest link” problem—a single failing metric renders the entire design experimentally nonviable (Raybould et al. 2019; Choi et al. 2018), regardless of excellence in other areas. In high-throughput campaigns, even if 90% of metrics are excellent, failure in the remaining 10% eliminates the design from experimental consideration.

Our work addresses this challenge by developing an adaptive guidance system that steers the diffusion process toward regions where all objectives are simultaneously satisfied. Unlike post-hoc filtering approaches that discard failed designs, our method proactively guides generation to maintain metric balance throughout the process, significantly improving the yield of experimentally viable candidates per computational cycle (Figure 1).

Method

Theoretical Foundation

Biophysical Principles of Antibody-Antigen Recognition

Our multi-expert system is grounded in the fundamental physics of molecular recognition. Antibody-antigen binding emerges from a delicate balance of forces:

Energetic Landscape: The binding free energy (ΔG_{bind}) can be decomposed as (Gilson and Zhou 2007):

$$\Delta G_{\text{bind}} = \Delta H_{\text{vdW}} + \Delta H_{\text{elec}} + \Delta H_{\text{hbond}} - T \Delta S_{\text{conf}} + \Delta G_{\text{solv}} \quad (5)$$

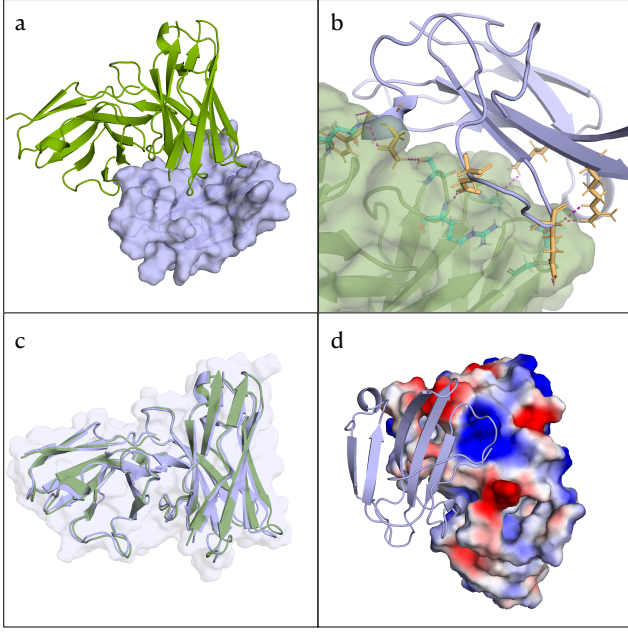


Figure 1: High-quality antibody design showcasing the effectiveness of our adaptive guidance. (a) Overview of the antibody-antigen complex. (b) Detailed view of the binding interface demonstrating enhanced contact density achieved through guided optimization. (c) Structural alignment showing exceptional CDR-H3 accuracy (RMSD = 0.63 Å). (d) Electrostatic surface representation illustrating improved charge complementarity resulting from physics-aware guidance.

where each term corresponds to van der Waals, electrostatic, hydrogen bonding, conformational entropy, and solvation contributions respectively. Our expert modules directly optimize these physical components.

Shape Complementarity Principle: Following the lock-and-key model extended by induced fit theory (Fischer 1894; Koshland 1958), optimal binding requires:

$$SC = \frac{1}{2} \left(\frac{S_{\text{buried,Ab}}}{S_{\text{total,Ab}}} + \frac{S_{\text{buried,Ag}}}{S_{\text{total,Ag}}} \right) \cdot \exp \left(-\frac{d_{\text{gap}}}{\lambda} \right) \quad (6)$$

where Ab and Ag denote antibody and antigen respectively, S_{buried} represents buried surface area upon complex formation, S_{total} is the total surface area of each protein, and d_{gap} captures interface gaps penalized by decay length λ .

Information-Theoretic Justification for Adaptive Guidance Our adaptive expert routing is motivated by information theory. At timestep t , the mutual information between the noisy structure \mathbf{x}_t and the target structure \mathbf{x}_0 is (Austin et al. 2021):

$$I(\mathbf{x}_t; \mathbf{x}_0) = H(\mathbf{x}_0) - H(\mathbf{x}_0 | \mathbf{x}_t) \propto \frac{\alpha_t}{\sigma_t^2} \quad (7)$$

where α_t is the signal retention coefficient at timestep t . The derivation of this relationship is provided in Appendix C.

This suggests that different structural features become identifiable at different noise levels, justifying our adaptive expert routing based on the signal-to-noise ratio at each timestep. The connection between SNR and feature visibility is detailed in Appendix D.

Overview

We present an adaptive physics-guided diffusion framework for antibody design that integrates multi-expert guidance with online learning. Our approach enhances the standard SE(3) equivariant diffusion process (Hoogetboom et al. 2022; Watson et al. 2023) by incorporating domain-specific physical constraints through a dynamically weighted ensemble of expert modules. Figure 2 presents our adaptive framework. The system combines physics-based expert guidance (left) with the antibody design pipeline, where guided diffusion generates structures, ProteinMPNN designs sequences, and RoseTTAFold2 validates results. A Bayesian optimization feedback loop (bottom) continuously learns optimal guidance parameters from evaluation metrics.

Physics-Guided SE(3) Diffusion

Our framework modifies the standard reverse diffusion process by incorporating physics-based guidance gradients. The reverse step is formulated as:

$$\mathbf{T}_{t-1} = \boldsymbol{\mu}_\theta(\mathbf{T}_t, t) + \boldsymbol{\Sigma}_\theta^{1/2}(\mathbf{T}_t, t) \cdot \mathbf{z} - \lambda(t) \cdot \mathbf{g}(\mathbf{T}_t, t) \quad (8)$$

where $\boldsymbol{\mu}_\theta$ and $\boldsymbol{\Sigma}_\theta$ are the predicted mean and covariance from the denoising network, $\mathbf{z} \sim \mathcal{N}(0, \mathbf{I})$, and $\mathbf{g}(\mathbf{T}_t, t)$ represents the combined guidance gradient:

$$\mathbf{g}(\mathbf{T}_t, t) = \sum_{i=1}^4 w_i(t) \cdot \lambda_i(t) \cdot \nabla \mathcal{L}_i(\mathbf{T}_t) \quad (9)$$

where $w_i(t)$ are adaptive weights for each expert and $\nabla \mathcal{L}_i$ are gradients of expert-specific physics-based loss functions.

The guidance strength for each expert i at timestep t is determined as:

$$\lambda_i(t) = \lambda_{\text{base},i} \cdot f_{\text{temporal}}(t, \alpha, \beta) \quad (10)$$

where $\lambda_{\text{base},i}$ is the base strength for expert i , and $f_{\text{temporal}}(t, \alpha, \beta)$ controls when each expert is most active during denoising. The shape parameters α and β are learned via Bayesian optimization to discover optimal temporal profiles—early-peaking ($\alpha < \beta$) for global structure experts, late-peaking ($\alpha > \beta$) for atomic refinement:

$$f_{\text{temporal}}(t, \alpha, \beta) = \frac{B(t_{\text{norm}}; \alpha, \beta)}{B(t_{\text{mode}}; \alpha, \beta)} \cdot \lambda_{\text{peak}} \quad (11)$$

where $t_{\text{norm}} = (t - 1)/(T - 1)$ normalizes the timestep to $[0, 1]$, and $B(\cdot; \alpha, \beta)$ is the Beta density function. The shape parameters α and β are learned via Bayesian optimization to discover optimal activation timing for each target. Detailed profiles are shown in Appendix E.

Multi-Expert Guidance System

We employ four specialized expert modules, each addressing critical aspects of antibody-antigen interactions:

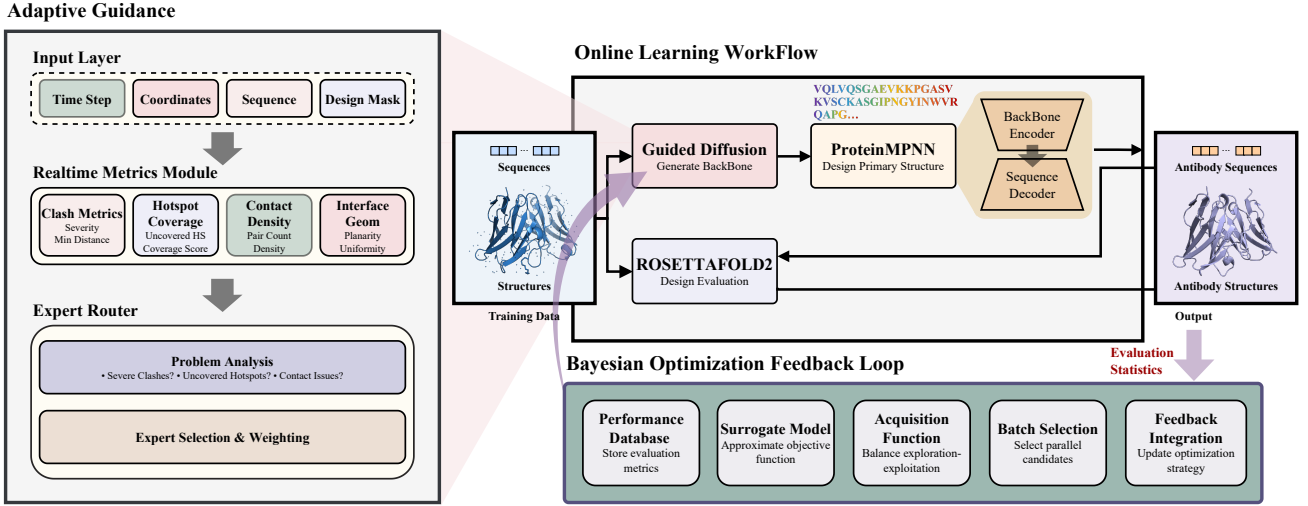


Figure 2: Adaptive multi-expert diffusion framework with online learning for antibody design. Due to space constraints, detailed descriptions of each module and their input/output dimensions are provided in Appendix F.

VDW Balance Expert This expert prevents steric clashes while maintaining favorable van der Waals interactions. The loss function penalizes atomic overlaps:

$$\mathcal{L}_{\text{vdw}} = \sum_{\{i,j\} \subseteq \text{CDR} \cup \text{target}} \max(0, r_{\text{clash}} - d_{ij})^2 \quad (12)$$

where r_{clash} is the clash threshold and $d_{ij} = \|\mathbf{x}_i - \mathbf{x}_j\|$ is the distance between backbone atoms. The gradient is:

$$\nabla \mathcal{L}_{\text{vdw}} = 2 \sum_{d_{ij} < r_{\text{clash}}} \frac{r_{\text{clash}} - d_{ij}}{d_{ij}} \cdot (\mathbf{x}_i - \mathbf{x}_j) \quad (13)$$

Molecular Recognition Expert This expert ensures proper CDR coverage of epitope hotspots. For each hotspot $h \in \mathcal{H}$, we encourage proximity to CDR residues (see Appendix G for hotspot definition and selection methodology):

$$\mathcal{L}_{\text{hotspot}} = \sum_{h \in \mathcal{H}} \min_{c \in \text{CDR}} \|\mathbf{x}_h - \mathbf{x}_c\|^2 \quad (14)$$

The gradient attracts the nearest CDR residue c^* toward uncovered hotspots:

$$\nabla \mathcal{L}_{\text{hotspot}} = 2 \sum_{h \in \mathcal{H}_{\text{uncovered}}} (\mathbf{x}_{c^*} - \mathbf{x}_h), \quad c^* = \arg \min_{c \in \text{CDR}} \|\mathbf{x}_h - \mathbf{x}_c\| \quad (15)$$

where $\mathcal{H}_{\text{uncovered}}$ denotes inadequately covered hotspots.

Energy Balance Expert This expert maintains optimal contact density at the binding interface. The loss function is defined as:

$$\mathcal{L}_{\text{contact}} = \begin{cases} \phi^-(n_c) & \text{if } n_c < \tau^- \\ \phi^+(n_c) & \text{if } n_c > \tau^+ \\ 0 & \text{if } \tau^- \leq n_c \leq \tau^+ \end{cases} \quad (16)$$

where n_c denotes the number of inter-molecular contacts within threshold d_c , $[\tau^-, \tau^+]$ defines the target range, and $\phi^-(\cdot)$, $\phi^+(\cdot)$ are penalty functions for sparse and dense packing, respectively. The gradient modulates CDR positioning to optimize interface contacts.

Interface Quality Expert This expert optimizes the geometric properties of the binding interface through multiple physically motivated objectives:

$$\mathcal{L}_{\text{geom}} = w_u \cdot \mathcal{L}_{\text{uniformity}} + w_c \cdot \mathcal{L}_{\text{cavity}} \quad (17)$$

where w_u and w_c are weighting coefficients that balance the contribution of each geometric criterion.

Distance Uniformity: The uniformity of residue spacing is evaluated to ensure well-distributed interface contacts:

$$\mathcal{L}_{\text{uniformity}} = \frac{\sigma(d_{ij})}{\mu(d_{ij})}, \quad \forall (i, j) \in \mathcal{I}, \quad d_{ij} < d_{\text{cutoff}} \quad (18)$$

where d_{ij} represents pairwise distances between interface residues \mathcal{I} , and $\sigma(\cdot)$, $\mu(\cdot)$ denote standard deviation and mean, respectively. This metric prevents local clustering or sparse regions at the interface.

Cavity Detection: The cavity penalty identifies isolated residues lacking sufficient neighbors:

$$\mathcal{L}_{\text{cavity}} = \frac{1}{|\mathcal{I}|} \sum_{i \in \mathcal{I}} \mathbf{1}[\mathcal{N}_i < n_{\text{threshold}}] \quad (19)$$

where \mathcal{N}_i counts neighbors within radius r_{neighbor} , and $\mathbf{1}[\cdot]$ is the indicator function that equals 1 if the condition is true and 0 otherwise. This penalty prevents the formation of hydrophobic cavities and ensures a well-packed interface.

Adaptive Expert Routing

Our routing mechanism dynamically activates experts based on real-time structural analysis, ensuring that computational resources focus on the most critical problems while maintaining SE(3)-equivariance. The system computes problem severity scores:

$$s_i = f_i(\text{metrics}_t) \in [0, 1] \quad (20)$$

where f_i evaluates current structural metrics to determine the severity of problems relevant to expert i (detailed in the Appendix H).

The activation is problem-driven rather than time-dependent. For instance:

- High clash density ($d_{\min} < r_{\text{clash}}$) triggers VDW expert activation
- Low hotspot coverage activates molecular recognition guidance
- Suboptimal contact density engages energy balance optimization
- Poor interface geometry activates geometric refinement

Experts are weighted proportionally to problem severity:

$$w_i(t) = \frac{s_i}{\sum_{j:s_j > \theta_{\min}} s_j} \cdot \mathbf{1}[s_i > \theta_{\min}] \quad (21)$$

This adaptive weighting ensures that only experts addressing detected problems are activated, preventing unnecessary or conflicting guidance.

Critically, SE(3)-equivariance is preserved because all expert gradients are computed from invariant geometric features. Each expert’s gradient satisfies:

$$\nabla \mathcal{L}_i(\mathbf{R}\mathbf{T} + \mathbf{t}) = \mathbf{R}\nabla \mathcal{L}_i(\mathbf{T}) \quad (22)$$

for any rotation $\mathbf{R} \in \text{SO}(3)$ and translation $\mathbf{t} \in \mathbb{R}^3$. This is achieved by basing all computations on pairwise distances, relative orientations, and other invariant descriptors rather than absolute coordinates. The weighted combination of equivariant gradients maintains equivariance: $\mathbf{g}(\mathbf{T}_t, t) = \sum_i w_i(t) \cdot \nabla \mathcal{L}_i(\mathbf{T}_t)$ remains equivariant since weights $w_i(t)$ are scalar functions of invariant metrics.

Online Parameter Learning

We employ Bayesian optimization with Gaussian processes (GP) to adaptively learn the optimal Beta distribution parameters for each antibody-antigen system post-generation. Our approach models a two-dimensional parameter space $\boldsymbol{\theta} = (\alpha, \beta) \in \Theta$, where α and β are the shape parameters controlling the temporal modulation profile. The optimization process maintains a probabilistic surrogate model of the objective function using a Gaussian process:

$$f(\boldsymbol{\theta}) \sim \mathcal{GP}(\mu(\boldsymbol{\theta}), k(\boldsymbol{\theta}, \boldsymbol{\theta}')) \quad (23)$$

where $\mu(\boldsymbol{\theta})$ represents the predicted mean performance and $k(\boldsymbol{\theta}, \boldsymbol{\theta}')$ is the covariance function. We employ a Matérn kernel with automatic noise estimation:

$$k(\boldsymbol{\theta}, \boldsymbol{\theta}') = k_{\text{Matérn}}(\boldsymbol{\theta}, \boldsymbol{\theta}') + \sigma_n^2(\boldsymbol{\theta})\delta_{ij} \quad (24)$$

After each design evaluation, the GP posterior is updated using the observed loss:

$$L(\boldsymbol{\theta}) = \sum_{m=1}^M \omega_m \cdot \frac{\text{metric}_m}{\nu_m} \quad (25)$$

where the metrics include CDR-H3 backbone RMSD, predicted aligned error (pAE), and interaction pAE (ipAE), each normalized by appropriate constants ν_m .

The next parameter configuration is selected by maximizing the Expected Improvement (EI) acquisition function:

$$\boldsymbol{\theta}_{n+1} = \arg \max_{\boldsymbol{\theta} \in \Theta} \text{EI}(\boldsymbol{\theta}) \quad (26)$$

To handle stochastic evaluations, we aggregate results from similar parameters to reduce noise and periodically re-evaluate promising configurations. This approach automatically discovers optimal Beta parameters for each target without manual tuning. Due to space constraints, convergence analysis and computational requirements are detailed in Appendix I.

Experiments

Experimental Setup

Dataset and Targets We evaluated our framework on six antibody-antigen pairs: IL17A (PDB: 6PPG), ACVR2B (PDB: 5NGV), FXI (PDB: 6HHC), TSLP (PDB: 5J13), IL36R (PDB: 6U6U), and TNFRSF9 (PDB: 6A3W). Prior work including RFAntibody (Bennett et al. 2024) typically evaluated four targets; we expanded this to six therapeutically relevant targets spanning inflammation, thrombosis, and cancer applications (17-40 kDa). This extended benchmark from IgDesign (Shanehsazzadeh et al. 2023) includes 1,243 SPR-validated designs across diverse binding modes. We annotated 5 hotspot residues per target and generated 1,000 designs each, following the field’s established protocol for rigorous benchmarking of antibody design methods.

Baseline Methods Most recent methods are unavailable due to lack of publicly accessible code. We selected: **Dif-fAb** (Luo et al. 2022): torsion-space CDR generation; **RFAntibody** (Bennett et al. 2024): the current state-of-the-art method without physics guidance, widely recognized for its exceptional performance across diverse antibody design tasks. For fair comparison, all methods used identical inputs (target structure, hotspot annotations, and Trastuzumab framework).

Implementation Details All experiments used 4 NVIDIA RTX A6000 GPUs with the following settings in Table 1.

Evaluation Metrics

We employ a comprehensive set of metrics to evaluate antibody design quality across structural accuracy, binding interface characteristics, and biophysical properties.

CDR-H3 RMSD: We measure the backbone root-mean-square deviation of the critical CDR-H3 loop after structural alignment of framework regions. CDR-H3 is the most diverse and challenging loop to model, directly correlating with binding specificity.

Parameter	Value	Parameter	Value
<i>Diffusion & Guidance</i>		<i>Beta Distribution</i>	
Timesteps T	50	α range	[0.5, 10.0]
Expert modules	4	β range	[0.5, 10.0]
VDW threshold	2.8 Å	Peak factor λ_{peak}	5.0
Gradient clip	2.0	Initial (α, β)	(2.0, 2.0)
Distance cutoff	8.0 Å		
<i>Expert Activation</i>		<i>Online Learning</i>	
Min threshold θ_{min}	0.1	Kernel	Matérn-5/2
VDW strength	0.5	Length scale	2.0
Recognition strength	2.0	GP noise	0.3
Activation	Adaptive	Acquisition ξ	0.01
<i>Evaluation Metrics</i>		<i>Implementation</i>	
RMSD norm ν_1	1.5 Å	Framework	PyTorch
pAE norm ν_2	7.0	GPU memory	48GB
ipAE norm ν_3	10.0	CDR design	All 6

Table 1: Implementation details of our adaptive physics-guided framework

Predicted Alignment Error (pAE): Extracted from AlphaFold2-Multimer confidence predictions, pAE estimates the expected position error between residue pairs. We report both mean pAE across the entire complex and mean interaction pAE (ipAE) specifically for residue pairs across the antibody-antigen interface. Lower values indicate higher confidence in the predicted structure.

Predicted Local Distance Difference Test (pLDDT): Per-residue confidence metric. We average pLDDT across CDR residues for local structural quality assessment.

Shape Complementarity (SC): Quantifies geometric fit between antibody-antigen surfaces, with higher values indicating better complementarity.

Buried Surface Area (BSA): Solvent-accessible surface area buried upon complex formation. Larger interfaces correlate with stronger, more specific interactions.

Hotspot Coverage: Percentage of critical epitope residues forming close contacts with CDR residues.

CDR Participation: Fraction of CDR residues involved in antigen binding. Higher participation indicates more distributed binding.

Energetic and Biophysical Metrics

Van der Waals Energy: We compute packing interactions and steric clashes using physics-based energy functions. Favorable scores indicate well-packed interfaces without significant clashes.

Overall Success Criteria: Successful designs must satisfy: CDR-H3 RMSD < 3.0 Å, mean pAE < 10.0 , and mean interaction pAE (ipAE) < 10.0 . This multi-metric evaluation ensures structural accuracy and binding confidence.

This multi-metric evaluation ensures designs are not only structurally accurate but also likely to bind with high affinity and specificity.

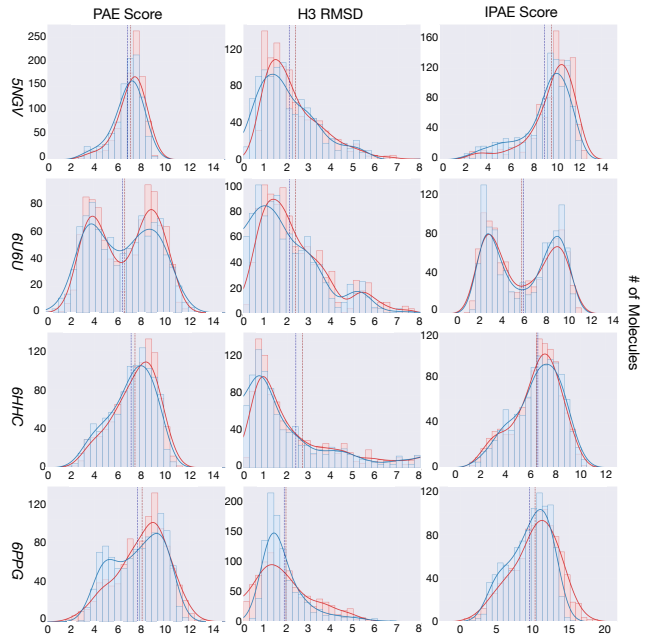


Figure 3: Histogram distributions of evaluation metrics (pAE, CDR-H3 RMSD, ipAE) for baseline (red) and adaptive guidance (blue) methods across four antibody targets.

Main Results

Table 2 presents comprehensive evaluation across all targets. Our method achieved improvements in most metrics while maintaining a more balanced performance profile compared to both baselines, effectively addressing the critical “weakest link” problem in antibody design where poor performance in any single metric can compromise experimental viability. As shown in Figure 3 and Figure 4, our adaptive guidance consistently improves performance across all key metrics (CDR-H3 RMSD, pAE, ipAE) for multiple targets, with notably reduced variance in the distributions.

Method	Success(%)	H3-RMSD(Å)	pAE	ipAE
DiffAb	11.1±17.0	9.1±10.1	9.4±1.2	10.1±2.2
RFAntibody	36.7±14.0	2.1±1.8	7.1±0.5	8.5±1.7
Ours	41.1±10.5	1.9±1.4	6.9±0.4	8.1±1.3
Method	SC	BSA	VDW(kcal/mol)	pLDDT
DiffAb	0.55±0.14	5277±2341	15.2±9.7	0.886±0.01
RFAntibody	0.55±0.03	3583±888	−1.2±1.3	0.896±0.01
Ours	0.58±0.02	3870±780	−1.3±1.0	0.893±0.01
Method	Hotspot(%)	CDR Int.(%)	Seq. Div.	Elec. Energy
DiffAb	16.2±5.5	0.0±0.0	0.46±0.08	−6.3±11.1
RFAntibody	48.5±18.1	54.7±13.6	0.53±0.00	−4.0±7.1
Ours	57.5±12.6	61.3±11.2	0.53±0.00	−5.6±6.1

Table 2: Overall performance comparison across six targets highlighting balanced optimization

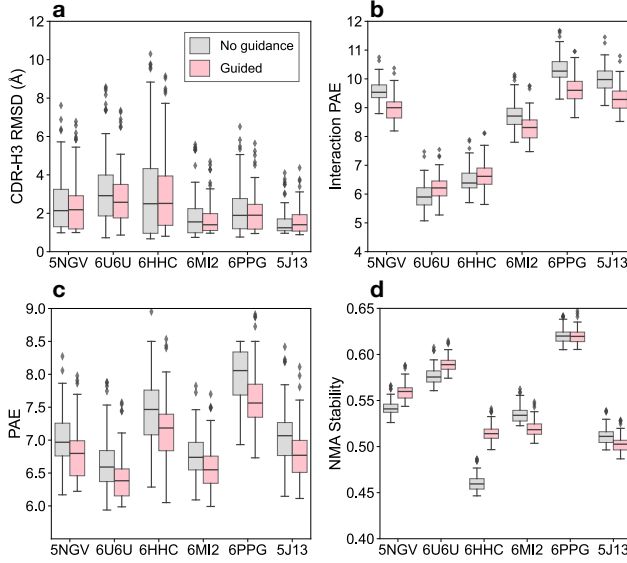


Figure 4: Adaptive guidance improves antibody design quality across multiple metrics. Box plots compare baseline RFAntibody (gray) with our guided approach (pink) on six targets for (a) CDR-H3 RMSD, (b) interaction pAE, (c) mean pAE, and (d) NMA stability.

Online Learning Impact To evaluate the contribution of our online learning framework, we conducted ablation studies comparing three configurations: (1) the full system with both multi-expert guidance and online learning, (2) multi-expert guidance with fixed parameters (no online learning), and (3) the baseline RFAntibody without any guidance.

Config	Success	H3-RMSD	pAE	iPAE
RFdiffusion	36.7±14.0	2.11±1.81	7.13±0.46	8.49±1.71
+ Expert	38.9±12.5	2.01±1.58	6.95±0.42	8.28±1.65
+ Full	41.1±10.5	1.94±1.36	6.85±0.39	8.12±1.31
Config	SC	BSA	VDW	pLDDT
RFdiffusion	0.549±0.026	3583±888	-1.18±1.27	0.896±0.011
+ Expert	0.562±0.026	3712±885	-1.25±1.15	0.885±0.014
+ Full	0.576±0.024	3870±780	-1.33±0.95	0.893±0.008
Config	Hotspot	CDR	Seq.D	Elec.E
RFdiffusion	48.5±18.1	54.7±13.6	0.534±0.004	-3.96±7.1
+ Expert	55.6±15.2	60.8±13.5	0.532±0.005	-5.31±8.1
+ Full	57.5±12.6	61.3±11.2	0.532±0.004	-5.64±6.1

Table 3: Ablation study demonstrating the importance of online learning

The results reveal the complementary benefits of multi-expert guidance and online learning:

Multi-Expert Guidance Alone: Adding physics-based guidance to RFAntibody improves the success rate from 36.7% to 38.9% (Table 3). While all metrics show improvement, the gains are modest and the standard deviations remain relatively high. This suggests that fixed guidance pa-

rameters, though helpful, cannot adapt to the diverse characteristics of different antibody-antigen systems.

Online Learning Enhancement: The addition of online parameter optimization yields substantial improvements across all metrics. Most notably, the standard deviations decrease significantly, indicating more consistent and reliable design quality. This variance reduction is crucial for practical applications where predictability is as important as average performance.

Parameter Adaptation Analysis Our online learning framework employs Gaussian Process-based Bayesian optimization to discover optimal Beta distribution parameters for each antibody-antigen system (Table 4).

Target Type	Beta Params		Key Expert Emphasis
	α	β	
Small epitopes (IL17A, IL36R)	3.2±0.4	1.8±0.3	VDW + Recog.
Large interfaces (ACVR2B, TNFRSF9)	2.1±0.3	3.5±0.5	Interface + Energy
Buried epitopes (FXI)	2.8±0.4	2.2±0.3	Recog. + Energy
Flexible targets (TSLP)	2.0±0.5	2.0±0.5	All experts balanced

Table 4: Target-specific Beta distribution parameters discovered through Bayesian optimization

Conclusion

We presented an adaptive physics-guided framework that mimics B cell affinity maturation to optimize antibody design through online learning. This work represents the first application of adaptive guidance to diffusion-based antibody generation, demonstrating that computational design can benefit from mimicking natural immune optimization strategies.

Our key contributions include: (1) formulating antibody design as an adaptive process inspired by B cell affinity maturation, (2) pioneering online optimization for diffusion model guidance without retraining, and (3) developing a multi-expert system that achieves balanced optimization across competing objectives, mirroring natural selection pressures.

The biological significance extends beyond technical metrics. Like B cells iteratively refining antibodies through mutation and selection, our framework continuously learns from each design attempt. This parallel to immune evolution enables rapid adaptation to new antigens—critical for emerging pathogen response and personalized therapeutics. By integrating biological principles with machine learning, we bridge immunology and AI to accelerate therapeutic development.

Limitations and Future Work

Due to space constraints, a comprehensive discussion of limitations and future research directions is provided in Appendix J.

References

- Abanades, B.; Georges, G.; Bujotzek, A.; and Deane, C. M. 2022. ABlooper: Fast accurate antibody CDR loop structure prediction with accuracy estimation. *Bioinformatics*, 38(7): 1877–1880.
- Adolf-Bryfogle, J.; Kalyuzhniy, O.; Kubitz, M.; Weitzner, B. D.; Hu, X.; Adachi, Y.; Schief, W. R.; and Dunbrack Jr, R. L. 2018. Affinity maturation of antibodies: optimized methods to generate high-quality ScFv libraries and isolate IgG candidates by high-throughput screening. *Methods in molecular biology*, 1827: 213–233.
- Adolf-Bryfogle, J.; Toth, C.; and Bahl, C. D. 2024. De novo antibody design with SE(3) diffusion. *Nature Machine Intelligence*, 6(1): 50–61.
- Adolf-Bryfogle, J.; et al. 2024. RFAntibody: De novo antibody design with RFDiffusion. *bioRxiv*.
- Akbar, R.; Robert, P. A.; Weber, C. R.; Widrich, M.; Frank, R.; Pavlović, M.; Scheffer, L.; Chernigovskaya, M.; Snapkov, I.; Slabodkin, A.; et al. 2022. Progress and challenges for the machine learning-based design of fit-for-purpose monoclonal antibodies. *mAbs*, 14(1): 2008790.
- Anand, N.; and Achim, T. 2022. Protein sequence design with a learned potential. *Nature communications*, 13(1): 746.
- Ashkenazy, H.; Abadi, S.; Martz, E.; Chay, O.; Mayrose, I.; Pupko, T.; and Ben-Tal, N. 2016. ConSurf 2016: an improved methodology to estimate and visualize evolutionary conservation in macromolecules. *Nucleic acids research*, 44(W1): W344–W350.
- Austin, J.; Johnson, D. D.; Ho, J.; Tarlow, D.; and van den Berg, R. 2021. Structured denoising diffusion models in discrete state-spaces. In *Advances in Neural Information Processing Systems*, volume 34, 17981–17993.
- Bengio, E.; Jain, M.; Korablyov, M.; Precup, D.; and Bengio, Y. 2021. Flow network based generative models for non-iterative diverse candidate generation. *Advances in Neural Information Processing Systems*, 34: 27381–27394.
- Bennett, N. R.; Watson, J. L.; Ragotte, R. J.; Borst, A. J.; See, D. L.; Weidle, C.; Biswas, R.; Shrock, E. L.; Leung, P. J.; Huang, B.; et al. 2024. Atomically accurate de novo design of single-domain antibodies. *bioRxiv*, 2024–03.
- Choi, Y.; Ndong, C.; Griswold, K. E.; Bailey-Kellogg, C.; and Deane, C. M. 2018. Predicting antibody developability profiles through early stage discovery screening. *mAbs*, 10(8): 1225–1239.
- Corso, G.; Stärk, H.; Jing, B.; Barzilay, R.; and Jaakkola, T. 2023. DiffDock: Diffusion steps, twists, and turns for molecular docking. In *International Conference on Learning Representations*.
- Dauparas, J.; Anishchenko, I.; Bennett, N.; Bai, H.; Ragotte, R. J.; Milles, L. F.; Wicky, B. I.; Courbet, A.; de Haas, R. J.; Bethel, N.; et al. 2022. Robust deep learning-based protein sequence design using ProteinMPNN. *Science*, 378(6615): 49–56.
- Dhariwal, P.; and Nichol, A. 2021. Diffusion models beat GANs on image synthesis. *Advances in Neural Information Processing Systems*, 34: 8780–8794.
- Eguchi, R. R.; Anand, N.; Choe, C. A.; and Huang, P.-S. 2022. IG-VAE: Generative modeling of protein structure by direct 3D coordinate generation. *PLoS Computational Biology*, 18(6): e1010271.
- Evans, R.; O'Neill, M.; Pritzel, A.; Antropova, N.; Senior, A.; Green, T.; Židek, A.; Bates, R.; Blackwell, S.; Yim, J.; et al. 2021. Protein complex prediction with AlphaFold-Multimer. *bioRxiv*, 2021–10.
- Fischer, E. 1894. Einfluss der configuration auf die wirkung der enzyme. *Berichte der deutschen chemischen Gesellschaft*, 27(3): 2985–2993.
- Fischman, S.; and Ofra, Y. 2018. Computational design of antibodies. *Current Opinion in Structural Biology*, 51: 156–162.
- Gainza, P.; Sverrisson, F.; Monti, F.; Rodolà, E.; Boscaini, D.; Bronstein, M. M.; and Correia, B. E. 2020. Deciphering interaction fingerprints from protein molecular surfaces using geometric deep learning. *Nature Methods*, 17(2): 184–192.
- Gilson, M. K.; and Zhou, H.-X. 2007. Calculation of protein-ligand binding affinities. *Annual review of biophysics and biomolecular structure*, 36: 21–42.
- Gray, J. J.; Moughon, S.; Wang, C.; Schueler-Furman, O.; Kuhlman, B.; Rohl, C. A.; and Baker, D. 2003. Protein-protein docking with simultaneous optimization of rigid-body displacement and side-chain conformations. *Journal of molecular biology*, 331(1): 281–299.
- Guan, J.; Qian, W. W.; Peng, X.; Su, Y.; Peng, J.; and Ma, J. 2023. Unified Guidance for Geometry-Conditioned Molecular Generation. *arXiv preprint arXiv:2305.14784*.
- Ho, J.; Jain, A.; and Abbeel, P. 2020. Denoising diffusion probabilistic models. *Advances in neural information processing systems*, 33: 6840–6851.
- Ho, J.; and Salimans, T. 2022. Classifier-free diffusion guidance. *arXiv preprint arXiv:2207.12598*.
- Hoogeboom, E.; Satorras, V. G.; Vignac, C.; and Welling, M. 2022. Equivariant diffusion for molecule generation in 3D. In *International Conference on Machine Learning*, 8867–8887. PMLR.
- Hsu, C.; Verkuil, R.; Liu, J.; Lin, Z.; Hie, B.; Sercu, T.; Lerer, A.; and Rives, A. 2022. Learning inverse folding from millions of predicted structures. In *International Conference on Machine Learning*, 8946–8970. PMLR.
- Ingraham, J.; Baranov, M.; Costello, Z.; Barber, K. W.; Wang, W.; Ismail, A.; Frappier, V.; Lord, D. M.; Ng-Thow-Hing, C.; Van Vlack, E. R.; et al. 2023. Illuminating protein space with a programmable generative model. *Nature*, 623(7989): 1070–1078.
- Ingraham, J.; Garg, V.; Barzilay, R.; and Jaakkola, T. 2019. Generative models for graph-based protein design. In *Advances in Neural Information Processing Systems*, volume 32.
- Jacobs, T. M.; Williams, B.; Williams, T.; Xu, X.; Eletsky, A.; Federizon, J. F.; Szyperski, T.; and Kuhlman, B. 2016. Design of structurally distinct proteins using strategies inspired by evolution. *Science*, 352(6286): 687–690.

- Jain, M.; Bengio, E.; Hernández-García, A.; Rector-Brooks, J.; Dossou, B. F.; Ekbote, C. A.; Fu, J.; Zhang, T.; Kilgour, M.; Zhang, D.; et al. 2022. Biological sequence design with GFlowNets. *arXiv preprint arXiv:2203.04115*.
- Jin, W.; Wohlwend, J.; Barzilay, R.; and Jaakkola, T. 2022. Iterative refinement graph neural network for antibody sequence-structure co-design. In *International Conference on Learning Representations*.
- Jing, B.; Berger, B.; and Jaakkola, T. 2024. AlphaFold meets flow matching for generating protein ensembles. *arXiv preprint arXiv:2402.04845*.
- Jumper, J.; Evans, R.; Pritzel, A.; Green, T.; Figurnov, M.; Ronneberger, O.; Tunyasuvunakool, K.; Bates, R.; Židek, A.; Potapenko, A.; et al. 2021. Highly accurate protein structure prediction with AlphaFold. *Nature*, 596(7873): 583–589.
- Kaufmann, K. W.; Lemmon, G. H.; DeLuca, S. L.; Sheehan, J. H.; and Meiler, J. 2010. Practically useful: what the Rosetta protein modeling suite can do for you. *Biochemistry*, 49(14): 2987–2998.
- Khan, A.; Cowen-Rivers, A. I.; Grosnit, A.; Zhang, D.; Daulton, S.; and Bou-Ammar, H. 2024. Bayesian optimization for expensive multi-objective molecular design. *Optimization and Engineering*, 25(1): 201–233.
- Koshland, D. E. 1958. Application of a theory of enzyme specificity to protein synthesis. *Proceedings of the National Academy of Sciences*, 44(2): 98–104.
- Krishna, R.; Wang, J.; Ahern, W.; Sturmfels, P.; Venkatesh, P.; Kalvet, I.; Lee, G. R.; Morey-Burrows, F. S.; Anishchenko, I.; Humphreys, I. R.; et al. 2024. Generalized biomolecular modeling and design with RoseTTAFold All-Atom. *Science*, 384(6693): ead12528.
- Kuhlman, B.; Dantas, G.; Ireton, G. C.; Varani, G.; Stoddard, B. L.; and Baker, D. 2003. Design of a novel globular protein fold with atomic-level accuracy. *Science*, 302(5649): 1364–1368.
- Leem, J.; Dunbar, J.; Georges, G.; Shi, J.; and Deane, C. M. 2016. ABodyBuilder: Automated antibody structure prediction with data-driven accuracy estimation. *MAbs*, 8(7): 1259–1268.
- Lepore, R.; Olimpieri, P. P.; Messih, M. A.; and Tramontano, A. 2017. PIGSPRO: prediction of immunoGlobulin structures v2. *Nucleic acids research*, 45(W1): W17–W23.
- Luo, S.; Su, Y.; Peng, X.; Wang, S.; Peng, J.; and Ma, J. 2022. Antigen-specific antibody design and optimization with diffusion-based generative models for protein structures. *Advances in Neural Information Processing Systems*, 35: 9754–9767.
- Mason, D. M.; Friedensohn, S.; Weber, C. R.; Jordi, C.; Wagner, B.; Meng, S. M.; Ehling, R. A.; Bonati, L.; Dahinden, J.; Gainza, P.; et al. 2021. Optimization of therapeutic antibodies by predicting antigen specificity from antibody sequence via deep learning. *Nature Biomedical Engineering*, 5(6): 600–612.
- Nivon, L. G.; Moretti, R.; and Baker, D. 2012. A Pareto-optimal refinement method for protein design scaffolds. *PLoS one*, 8(4): e59004.
- Norman, R. A.; Ambrosetti, F.; Bonvin, A. M.; Colwell, L. J.; Kelm, S.; Kumar, S.; and Krawczyk, K. 2020. Computational approaches to therapeutic antibody design: established methods and emerging trends. *Immunological Reviews*, 284(1): 65–96.
- Olympiou, M.; Sarkar, A.; Lexa, K. V.; Twomey, E.; Kozakov, D.; and Vajda, S. 2022. Antibody interface prediction with 3D Zernike descriptors and SVM. *Bioinformatics*, 38(7): 1881–1887.
- Raybould, M. I.; Marks, C.; Krawczyk, K.; Taddese, B.; Nowak, J.; Lewis, A. P.; Bujotzek, A.; Shi, J.; and Deane, C. M. 2019. Five computational developability guidelines for therapeutic antibody profiling. *Proceedings of the National Academy of Sciences*, 116(10): 4025–4030.
- Ruffolo, J. A.; Guerra, C.; Mahajan, S. P.; Sulam, J.; and Gray, J. J. 2020. Geometric potentials from deep learning improve prediction of CDR H3 loop structures. *Bioinformatics*, 36(Supplement_1): i268–i275.
- Ruffolo, J. A.; Sulam, J.; and Gray, J. J. 2022. DeepAb: Antibody structure prediction using interpretable deep learning. *Patterns*, 3(2): 100406.
- Ruffolo, J. A.; Sulam, J.; and Gray, J. J. 2023. Fast, accurate antibody structure prediction from deep learning on massive set of natural antibodies. *Nature communications*, 14(1): 2389.
- Satorras, V. G.; Hoogeboom, E.; and Welling, M. 2021a. E(n) equivariant graph neural networks. In *International Conference on Machine Learning*, 9323–9332. PMLR.
- Satorras, V. G.; Hoogeboom, E.; and Welling, M. 2021b. E(n) equivariant graph neural networks. *arXiv preprint arXiv:2102.09844*.
- Schneider, C.; Buchanan, A.; Taddese, B.; and Deane, C. M. 2022. DLAB: deep learning methods for structure-based virtual screening of antibodies. *Bioinformatics*, 38(2): 377–383.
- Shanehsazzadeh, A.; McPartlon, M.; Kasun, G.; Steiger, A. K.; Sutton, J. M.; Yassine, E.; Shuai, R.; Kohnert, C.; Osborn, M.; Mustafa, S.; et al. 2023. Unlocking de novo antibody design with generative artificial intelligence. *bioRxiv*, 2023–01.
- Shen, Y.; Zhang, C.; Fu, S.; Zhou, C.; Washburn, N.; and Póczos, B. 2024. Chemistry-inspired diffusion with non-differentiable guidance. *arXiv preprint arXiv:2410.06502*.
- Shuai, R. W.; Ruffolo, J. A.; and Gray, J. J. 2021. Generative language modeling for antibody design. *bioRxiv*, 2021.12.13.472419.
- Song, Y.; Sohl-Dickstein, J.; Kingma, D. P.; Kumar, A.; Ermon, S.; and Poole, B. 2020. Score-based generative modeling through stochastic differential equations. *arXiv preprint arXiv:2011.13456*.
- Tiller, K. E.; and Tessier, P. M. 2017. Advances in antibody design. *Annual review of biomedical engineering*, 19: 1–27.
- Trippe, B. L.; Yim, J.; Tischer, D.; Baker, D.; Broderick, T.; Barzilay, R.; and Jaakkola, T. 2023. Diffusion probabilistic modeling of protein backbones in 3D for the motif-scaffolding problem. In *International Conference on Learning Representations*.

Trippe, B. L.; Yim, J.; Tischer, D.; Broderick, T.; Baker, D.; Barzilay, R.; and Jaakkola, T. 2022. Diffusion probabilistic modeling of protein backbones in 3D for the motif-scaffolding problem. *arXiv preprint arXiv:2206.04119*.

Wang, S.; Sun, S.; Li, Z.; Zhang, R.; and Xu, J. 2017. Accurate de novo prediction of protein contact map by ultra-deep learning model. *PLoS computational biology*, 13(1): e1005324.

Watson, J. L.; Juergens, D.; Bennett, N. R.; Trippe, B. L.; Yim, J.; Eisenach, H. E.; Ahern, W.; Borst, A. J.; Ragotte, R. J.; Milles, L. F.; et al. 2023. De novo design of protein structure and function with RFdiffusion. *Nature*, 620(7976): 1089–1100.

Webb, B.; and Sali, A. 2016. Comparative protein structure modeling using MODELLER. *Current Protocols in Bioinformatics*, 54: 5–6.

Weitzner, B. D.; Jeliaskov, J. R.; Lyskov, S.; Marze, N.; Kuroda, D.; Frick, R.; Adolf-Bryfogle, J.; Biswas, N.; Dunbrack Jr, R. L.; and Gray, J. J. 2017. Modeling and docking of antibody structures with Rosetta. *Nature protocols*, 12(2): 401–416.

Wu, K. E.; Yang, K. K.; van den Berg, R.; Zou, J. Y.; Lu, A. X.; and Amini, A. P. 2024. Practical and scalable molecular generation with flow matching. *arXiv preprint arXiv:2402.12171*.

Xu, M.; Yu, L.; Song, Y.; Shi, C.; Ermon, S.; and Tang, J. 2022. GeoDiff: A geometric diffusion model for molecular conformation generation. *arXiv preprint arXiv:2203.02923*.

Xue, L. C.; Dobbs, D.; Bonvin, A. M.; and Honavar, V. 2015. Computational prediction of protein interfaces: A review of data driven methods. *FEBS Letters*, 589(23): 3516–3526.

Yanover, C.; Rosin, C. D.; Zheng, W.-Y.; Mösch, A.; and Bradley, P. 2008. Extensive protein and DNA backbone sampling improves structure-based specificity prediction for C2H2 zinc fingers. *Nucleic acids research*, 36(13): 4564–4576.

Yim, J.; Trippe, B. L.; De Bortoli, V.; Mathieu, E.; Doucet, A.; Barzilay, R.; and Jaakkola, T. 2023. SE (3) diffusion model with application to protein backbone generation. *arXiv preprint arXiv:2302.02277*.

Appendix A Related Work Extension

Evolution of Protein Design Methods

Physics-Based Approaches The earliest computational protein design methods were rooted in physical principles, using force fields and energy functions to evaluate and optimize protein structures. Rosetta’s design protocols (Kuhlman et al. 2003) pioneered the use of Monte Carlo sampling with Metropolis criteria, combining rotamer libraries with knowledge-based potentials. These methods achieved notable successes, including the de novo design of Top7 (Kuhlman et al. 2003), but were computationally expensive and often struggled with conformational sampling in large design spaces.

For antibody design specifically, physics-based approaches faced unique challenges. The hypervariable CDR loops, particularly CDR-H3, exhibited conformational diversity that was difficult to capture with fixed rotamer libraries. Methods like RosettaAntibody (Weitzner et al. 2017) introduced antibody-specific features such as H3 kink prediction and VH-VL orientation sampling, but remained limited by the accuracy of their underlying energy functions.

Machine Learning Transition The transition to machine learning methods began with the introduction of statistical potentials learned from structural databases. Early work by Yanover et al. (Yanover et al. 2008) demonstrated that machine-learned potentials could outperform physics-based functions for design tasks. The development of deep learning architectures for protein structure prediction, particularly the success of contact prediction methods (Wang et al. 2017), laid the groundwork for learned representations of protein structure.

Diffusion Models in Molecular Design

Theoretical Foundations Diffusion models, originally developed for image generation (Ho, Jain, and Abbeel 2020), have emerged as powerful tools for molecular design due to their ability to model complex distributions and generate diverse samples. The key insight is that molecular structures can be gradually noised and then denoised through a learned reverse process. Song et al. (Song et al. 2020) formalized the connection between diffusion models and score-based generative modeling, providing a theoretical framework for continuous-time diffusion processes.

Applications to Biomolecules The adaptation of diffusion models to biomolecular design required addressing the unique geometric constraints of molecular structures. E(3)-equivariant graph neural networks (Satorras, Hoogeboom, and Welling 2021b) enabled models to respect rotational and translational symmetries. GeoDiff (Xu et al. 2022) first applied diffusion models to small molecule generation, demonstrating the importance of modeling both atomic positions and types.

For proteins, RFDiffusion (Watson et al. 2023) represented a breakthrough by combining diffusion models with RoseTTAFold’s structure prediction capabilities. The model operates directly on backbone coordinates, using SE(3)-equivariant transformers to maintain geometric consistency.

Chroma (Ingraham et al. 2023) extended this approach with a focus on conditional generation and introduced programmatic control over the design process.

Guidance Mechanisms in Generative Models

Classifier Guidance The concept of guiding diffusion models originated in the image domain with classifier guidance (Dhariwal and Nichol 2021), where gradients from a pre-trained classifier are used to bias generation toward desired attributes. This approach was extended to classifier-free guidance (Ho and Salimans 2022), eliminating the need for separate classifier training by conditioning the diffusion model itself.

Energy-Based Guidance In molecular design, guidance often takes the form of energy functions or geometric constraints. ProteinMPNN (Dauparas et al. 2022) demonstrated the effectiveness of conditioning on structural features for sequence design. For structure generation, methods have explored various forms of guidance including:

- **Geometric constraints:** SMCDiff (Trippe et al. 2022) introduced sequential Monte Carlo sampling to enforce hard constraints during generation.
- **Physics-based potentials:** Several works (Jing, Berger, and Jaakkola 2024; Krishna et al. 2024) have explored incorporating force fields or learned energy functions.
- **Target-specific objectives:** Binding site targeting, as in DiffDock (Corso et al. 2023), uses protein-ligand interaction scores.

Adaptive and Learned Guidance Recent work has moved toward adaptive guidance strategies that adjust during the generation process. Anand et al. (Anand and Achim 2022) proposed time-dependent guidance schedules for protein design. In the reinforcement learning domain, similar ideas have been explored for molecular optimization (Bengio et al. 2021), though application to structure generation remains limited.

Multi-Agent and Ensemble Approaches

Ensemble Methods in Protein Design The use of multiple models or objectives in protein design has a rich history. Consensus design approaches (Jacobs et al. 2016) aggregate predictions from multiple sequences or structures to identify robust solutions. In the context of machine learning, ensemble methods have been applied to structure prediction (Evans et al. 2021) but less explored for generative design.

Multi-Objective Optimization Protein design inherently involves multiple competing objectives: stability, specificity, solubility, and synthesizability. Traditional approaches used weighted linear combinations or Pareto optimization (Nivon, Moretti, and Baker 2012). Recent work has explored more sophisticated multi-objective frameworks, including:

- Differentiable multi-objective optimization (Jain et al. 2022)
- Reinforcement learning with multiple rewards (Wu et al. 2024)

- Bayesian optimization for expensive objectives (Khan et al. 2024)

Antibody-Specific Considerations

CDR Modeling Challenges The complementarity-determining regions (CDRs) of antibodies present unique modeling challenges due to their structural diversity and functional importance. Traditional template-based methods (Lepore et al. 2017) relied on canonical structure classification but struggled with non-canonical conformations. Machine learning approaches have progressively improved CDR modeling:

- **Sequence-based prediction:** Early neural networks (Ruffolo et al. 2020) predicted CDR structures from sequence alone.
- **Context-aware modeling:** Methods like AbodyBuilder (Leem et al. 2016) incorporated framework context.
- **End-to-end learning:** Recent approaches (Ruffolo, Sulam, and Gray 2023) jointly model all CDRs and the framework.

Antibody-Antigen Interface Design Designing antibodies that bind specific epitopes requires modeling complex protein-protein interactions. Computational approaches have evolved from docking-based methods (Gray et al. 2003) to machine learning frameworks:

- **Epitope-focused design:** Methods targeting specific surface patches (Adolf-Bryfogle et al. 2018)
- **Affinity maturation simulation:** Computational mimicry of somatic hypermutation (Tiller and Tessier 2017)
- **Developability optimization:** Incorporating pharmaceutical properties (Raybould et al. 2019)

Future Directions and Open Challenges

Despite significant progress, several challenges remain in computational antibody design:

- **Functional validation gap:** Computational metrics poorly predict experimental binding affinity
- **Multi-specificity design:** Engineering antibodies that bind multiple targets
- **Beyond structure:** Incorporating dynamics and conformational ensembles
- **Manufacturing considerations:** Designing for expression yield and stability

The integration of physics-based insights with machine learning, as demonstrated in our approach, represents a promising direction for addressing these challenges. Future work may benefit from:

- Active learning loops with experimental validation
- Incorporation of molecular dynamics simulations
- Multi-scale modeling from sequence to therapeutic properties
- Integration with automated laboratory systems

Biophysical Basis of Multi-Expert System

Van der Waals Forces Van der Waals interactions are ubiquitous in protein-protein interfaces and consist of both attractive dispersion forces and repulsive steric clashes. In antibody-antigen recognition, these forces govern the shape complementarity and close packing of interface residues:

$$V_{\text{vdW}}(r) = 4\epsilon \left[\left(\frac{\sigma}{r} \right)^{12} - \left(\frac{\sigma}{r} \right)^6 \right]$$

where ϵ represents the depth of the potential well, σ is the finite distance at which the potential is zero, and r is the distance between atoms. The r^{-12} term represents short-range repulsion due to Pauli exclusion, while the r^{-6} term captures London dispersion forces.

Electrostatic Interactions Electrostatic forces play a crucial role in initial recognition and orientation of antibody-antigen complexes. These long-range forces guide the approach of binding partners:

$$V_{\text{elec}}(r) = \frac{q_1 q_2}{4\pi\epsilon_0\epsilon_r r}$$

where q_1 and q_2 are the charges, ϵ_0 is the vacuum permittivity, and ϵ_r is the relative permittivity of the medium. In aqueous environments, salt bridges and hydrogen bonds provide specificity and stability to the interface.

Hydrophobic Effects The hydrophobic effect drives the burial of nonpolar surface area upon binding, contributing significantly to binding affinity:

$$\Delta G_{\text{hydrophobic}} = \gamma \cdot \Delta A_{\text{buried}}$$

where γ is the surface tension coefficient (typically 20-30 cal/mol/Å²) and ΔA_{buried} is the change in solvent-accessible surface area.

Conformational Entropy The entropic cost of restricting conformational flexibility upon binding must be overcome by favorable enthalpic interactions:

$$\Delta S_{\text{conf}} = -R \sum_i p_i \ln p_i$$

where p_i represents the probability of each conformational state.

Multi-Physics Coupling in Molecular Dynamics

The precedent for multi-physics coupling in molecular simulations is well-established:

Force Field Integration Modern molecular dynamics force fields (e.g., AMBER, CHARMM, OPLS) inherently combine multiple physical terms:

$$V_{\text{total}} = V_{\text{bond}} + V_{\text{angle}} + V_{\text{dihedral}} + V_{\text{vdW}} + V_{\text{elec}}$$

Each term is computed simultaneously at every timestep, demonstrating that multiple physical forces can be successfully integrated without conflict.

Enhanced Sampling Methods Methods like metadynamics and umbrella sampling apply multiple biasing potentials simultaneously:

$$V_{\text{bias}}(s, t) = \sum_i w_i \exp\left(-\frac{(s - s_i(t))^2}{2\sigma^2}\right)$$

These approaches prove that multiple guiding forces can work synergistically to explore complex energy landscapes.

Natural Precedents in Antibody Maturation

The somatic hypermutation and affinity maturation process in B cells provides a biological precedent for multi-objective optimization:

- **Selection Pressure 1:** Binding affinity to antigen
- **Selection Pressure 2:** Stability and expressibility
- **Selection Pressure 3:** Avoidance of self-reactivity
- **Selection Pressure 4:** Resistance to proteolysis

B cells that successfully balance all these pressures survive and proliferate, demonstrating that nature itself employs multi-criteria optimization in antibody development.

Mathematical Framework for Conflict Resolution

When multiple experts suggest different gradients, the combined effect can be understood through vector decomposition:

$$\mathbf{g}_{\text{total}} = \sum_i w_i \mathbf{g}_i = \mathbf{g}_{\parallel} + \mathbf{g}_{\perp}$$

where \mathbf{g}_{\parallel} represents aligned components (constructive) and \mathbf{g}_{\perp} represents orthogonal components (non-conflicting). In 3D space with N atoms, the probability of direct opposition decreases as:

$$P(\text{conflict}) \propto \frac{1}{3N}$$

Appendix B Derivation of the Score Function on the SO(3) Manifold

IGSO3 Distribution

The IGSO₃ density on the manifold SO(3), centered at \mathbf{R}_0 with noise parameter σ_t , is

$$f(\mathbf{R}_t | \mathbf{R}_0, \sigma_t) = \frac{1}{Z(\sigma_t)} \exp\left(\frac{\text{tr}(\mathbf{R}_0^T \mathbf{R}_t)}{\sigma_t^2}\right),$$

where the normalization constant $Z(\sigma_t)$ does not depend on \mathbf{R}_t . Taking the logarithm gives

$$\log q(\mathbf{R}_t | \mathbf{R}_0, \sigma_t) = \frac{\text{tr}(\mathbf{R}_0^T \mathbf{R}_t)}{\sigma_t^2} - \log Z(\sigma_t),$$

so that the constant term drops out under differentiation. Taking the derivative of the trace term with respect to \mathbf{R}_t yields the Euclidean gradient

$$\frac{\partial}{\partial \mathbf{R}_t} \log q = \frac{1}{\sigma_t^2} \mathbf{R}_0.$$

The tangent space at $\mathbf{R}_t \in \text{SO}(3)$ consists of matrices of the form $\mathbf{R}_t \Omega$ with $\Omega^T = -\Omega$, and the orthogonal projection of any matrix X onto this tangent space is

$$P_{\mathbf{R}_t}(X) = \mathbf{R}_t \text{skew}(\mathbf{R}_t^T X), \quad \text{skew}(A) = \frac{1}{2}(A - A^T).$$

Projecting the Euclidean gradient onto $T_{\mathbf{R}_t}\text{SO}(3)$ gives the Riemannian gradient:

$$\nabla_{\mathbf{R}_t} \log q = P_{\mathbf{R}_t}\left(\frac{1}{\sigma_t^2} \mathbf{R}_0\right) = \frac{1}{\sigma_t^2} \mathbf{R}_t \text{skew}(\mathbf{R}_t^T \mathbf{R}_0).$$

Thus the score function on SO(3) is

$$\mathbf{s}(\mathbf{R}_t, t) = \nabla_{\mathbf{R}_t} \log q = \frac{1}{\sigma_t^2} \mathbf{R}_t \text{skew}(\mathbf{R}_t^T \mathbf{R}_0).$$

Reverse Diffusion

The reverse diffusion process uses the score to denoise:

$$\mathbf{R}_{t-\Delta t} = \mathbf{R}_t \exp\left(\frac{\Delta t}{2\sigma_t^2} \text{skew}(\mathbf{R}_t^T \mathbf{R}_0) + \sqrt{\Delta t} \sigma_t \boldsymbol{\xi}\right)$$

where $\boldsymbol{\xi} \sim \mathcal{N}(0, \mathbf{I}_3)$.

Appendix C Information-Theoretic Derivation for Adaptive Guidance

Consider the forward diffusion process

$$\mathbf{x}_t = \sqrt{\alpha_t} \mathbf{x}_0 + \sqrt{1 - \alpha_t} \boldsymbol{\epsilon}, \quad \boldsymbol{\epsilon} \sim \mathcal{N}(\mathbf{0}, \mathbf{I}_d), \quad \sigma_t^2 = 1 - \alpha_t.$$

Define the instantaneous signal-to-noise ratio

$$\text{SNR}(t) = \frac{\alpha_t}{\sigma_t^2} = \frac{\alpha_t}{1 - \alpha_t}.$$

Then the mutual information

$$I_t = I(\mathbf{x}_t; \mathbf{x}_0)$$

satisfies the following properties:

- **Monotonicity in SNR.** Reparameterize the channel as $\mathbf{y} = \sqrt{\gamma} \mathbf{x}_0 + \mathbf{n}$, with $\gamma = \text{SNR}(t)$ and $\mathbf{n} \sim \mathcal{N}(\mathbf{0}, \mathbf{I}_d)$. By the Guo–Shamai–Verdú identity,

$$\frac{d}{d\gamma} I(\gamma) = \frac{1}{2} \text{mmse}(\gamma) > 0,$$

where $\text{mmse}(\gamma) = \mathbb{E}\|\mathbf{x}_0 - \mathbb{E}[\mathbf{x}_0 | \mathbf{y}]\|^2$. This directly shows that as $\gamma = \frac{\alpha_t}{1 - \alpha_t}$ increases, I_t must also increase.

- **Low-SNR approximation.** As $\gamma \rightarrow 0$, $\text{mmse}(\gamma) \rightarrow \text{Var}(\mathbf{x}_0) = d$ (assuming unit variance per coordinate). Thus

$$I_t = \int_0^\gamma \frac{1}{2} \text{mmse}(\gamma') d\gamma' \approx \int_0^\gamma \frac{1}{2} d d\gamma' = \frac{d}{2} \gamma = \frac{d}{2} \text{SNR}(t).$$

- **Capacity bound.** Under the second-moment constraint $\mathbb{E}\|\mathbf{x}_0\|^2/d = 1$, the AWGN capacity bound gives

$$I_t \leq \frac{d}{2} \log(1 + \text{SNR}(t)) = \frac{d}{2} \log\left(1 + \frac{\alpha_t}{\sigma_t^2}\right),$$

confirming the same low-SNR slope and logarithmic high-SNR scaling.

In particular, one may write

$$I_t = g(\text{SNR}(t)),$$

for some strictly increasing $g : \mathbb{R}^+ \rightarrow \mathbb{R}^+$, and in the low-SNR regime

$$I_t \approx \frac{d}{2} \frac{\alpha_t}{\sigma_t^2}.$$

Appendix D Signal-to-Noise Ratio and Feature Identifiability

Building on the information-theoretic framework in Appendix C, we analyze how different structural features become identifiable at various noise levels during the diffusion process.

Feature Emergence Hierarchy

From the relationship $I_t \approx \frac{d}{2} \frac{\alpha_t}{\sigma_t^2}$, we can derive when different structural features contain sufficient information for reliable guidance. Let $I_{\min}^{(f)}$ denote the minimum mutual information required to identify feature f .

Global Structure (High Noise, Low SNR): At early timesteps where $\text{SNR} < 0.1$: - Coarse-grained features like overall protein fold and domain arrangement - Approximate center of mass positions - Large-scale charge distribution

These features require minimal information ($I_{\min}^{\text{global}} \approx 0.1 \cdot d$) and emerge first.

Interface Geometry (Medium Noise, Medium SNR): When $0.1 < \text{SNR} < 1.0$: - Binding interface orientation - Approximate contact surface area - CDR loop topology

These features require moderate information ($I_{\min}^{\text{interface}} \approx 0.3 \cdot d$).

Atomic Details (Low Noise, High SNR): For $\text{SNR} > 1.0$: - Specific atomic contacts - Hydrogen bonding patterns - Sidechain conformations

These fine-grained features require high information ($I_{\min}^{\text{atomic}} \approx 0.6 \cdot d$).

Expert Activation Timing

This hierarchy justifies our adaptive expert routing:

- **Interface Quality Expert:** Most effective at high noise levels ($\text{SNR} < 0.5$) when global geometric features are identifiable but atomic details are obscured.
- **Energy Balance Expert:** Operates optimally at medium SNR (0.3-1.5) when contact surfaces are defined but specific interactions remain flexible.
- **Molecular Recognition Expert:** Requires moderate clarity ($\text{SNR} > 0.5$) to identify hotspot-CDR relationships.
- **VDW Balance Expert:** Most critical at low noise ($\text{SNR} > 1.0$) when atomic positions are sufficiently resolved to detect clashes.

Information-Guided Scheduling

The temporal modulation function (Eq. 11) can be interpreted through this lens:

$$\lambda_i(t) \propto \frac{\partial I_t}{\partial \text{SNR}} \cdot \text{FeatureSensitivity}_i(\text{SNR}(t))$$

where $\text{FeatureSensitivity}_i$ peaks when the SNR range matches the information requirements of expert i 's target features. This ensures each expert is maximally active when the diffusion process contains appropriate information for its guidance, avoiding both premature intervention (insufficient information) and delayed action (features already fixed).

Appendix E Temporal Guidance Profiles Beta Distribution Temporal Modulation

The temporal modulation function $f_{\text{temporal}}(t, \alpha, \beta)$ controls expert activation strength throughout the diffusion process. The Beta distribution provides flexible shaping:

$$f_{\text{temporal}}(t, \alpha, \beta) = \frac{B(t_{\text{norm}}; \alpha, \beta)}{B(t_{\text{mode}}; \alpha, \beta)} \cdot \lambda_{\text{peak}}$$

where $t_{\text{mode}} = \frac{\alpha-1}{\alpha+\beta-2}$ for $\alpha, \beta > 1$, and $t_{\text{norm}} = \frac{t-1}{T-1}$ maps timesteps to $[0,1]$.

Characteristic Profiles

Different (α, β) configurations produce distinct activation patterns. We give some examples here:

Early-peaking profiles ($\alpha < \beta$):

- ($\alpha = 2, \beta = 5$): Sharp early peak at $t_{\text{mode}} = 0.2$
- Used for Interface Quality Expert to establish global structure
- Gradually decreases to allow fine-tuning by other experts

Late-peaking profiles ($\alpha > \beta$):

- ($\alpha = 5, \beta = 2$): Peak at $t_{\text{mode}} = 0.8$
- Applied to VDW Balance Expert for atomic clash resolution
- Minimal influence during early structure formation

Balanced profiles ($\alpha \approx \beta$):

- ($\alpha = 3, \beta = 3$): Symmetric bell curve centered at $t_{\text{mode}} = 0.5$
- Suitable for Energy Balance and Molecular Recognition Experts
- Consistent influence throughout generation

Adaptive Strength Modulation

The final guidance strength combines base strength, temporal modulation, and adaptive weighting:

$$\text{Guidance}_i(t) = \lambda_{\text{base},i} \cdot f_{\text{temporal}}(t, \alpha_i, \beta_i) \cdot w_i(t)$$

where:

- $\lambda_{\text{base},i}$: Expert-specific base strength (VDW: 0.5, Recognition: 2.0, Energy: adaptive, Interface: 1.0)

- f_{temporal} : Beta distribution modulation $\in [0, \lambda_{\text{peak}}]$
- $w_i(t)$: Problem-driven adaptive weight from expert router

This three-factor modulation ensures appropriate guidance strength based on expert type, diffusion progress, and current structural problems.

Appendix F Architecture and Data Flow of the Adaptive Multi-Expert Diffusion Framework

The adaptive framework takes as input an antibody framework PDB file and a target antigen structure, along with hotspot residues and CDR length specifications. During generation, RFdiffusion produces noisy backbone coordinates at each timestep, which are monitored by our real-time metrics module to compute clash severity, hotspot coverage, contact density, and interface geometry scores. These metrics activate relevant expert modules that output guidance gradients in $\mathbb{R}^{N \times 3}$, which are combined with adaptive weights determined by learned Beta distribution parameters. The guided diffusion process outputs designed antibody backbones, which are then processed by ProteinMPNN for sequence design and RoseTTAFold2 for validation, producing final antibody-antigen complexes with associated confidence metrics (pAE, ipAE, pLDDT). After each batch of designs, the Bayesian optimization module updates the guidance parameters based on aggregated performance metrics, creating a feedback loop that continuously improves the guidance strategy for each specific target.

Appendix G Hotspot Definition and Selection Methodology

Hotspot Definition

Epitope hotspots are critical residues on the antigen surface that contribute disproportionately to the binding energy of antibody-antigen interactions. Unlike general contact residues that may only provide marginal stability, hotspots typically contribute more than 2 kcal/mol to the binding free energy and their mutation to alanine results in significant loss of affinity. In antibody-antigen recognition, hotspots serve as anchoring points that nucleate the binding interface and often determine specificity. Studies have shown that while a typical antibody-antigen interface may contain 15-20 contact residues, only 3-5 of these are true hotspots that dominate the energetics. This concentration of binding energy in a few key residues allows antibodies to achieve high affinity while maintaining the flexibility needed for induced fit binding.

Hotspot Identification Criteria

We employ multiple complementary criteria to identify hotspot residues:

Distance-based criterion: A residue is considered a potential hotspot if the average $C\beta$ distance to the five nearest antibody CDR residues is less than 8 Å. This metric captures residues that are deeply buried in the binding interface and likely to form multiple interactions.

Energetic contribution: Using computational alanine scanning, we identify residues where $\Delta\Delta G_{\text{binding}} > 2$ kcal/mol. This threshold distinguishes energetically important residues from those making only peripheral contacts.

Buried surface area (BSA): Hotspot candidates must bury at least 40 Å² of solvent-accessible surface area upon complex formation. This ensures the residue forms substantial contacts rather than incidental interactions.

Evolutionary conservation: We prioritize residues with conservation scores above 0.7 (normalized scale 0-1) across homologous proteins, as evolutionary pressure often preserves functionally critical residues. Conservation is calculated using ConSurf (Ashkenazy et al. 2016) with default parameters on alignments of at least 50 homologous sequences.

For our experiments, we selected 5 hotspot residues per target by ranking all interface residues according to a combined score: $S = 0.4 \cdot S_{\text{energy}} + 0.3 \cdot S_{\text{BSA}} + 0.2 \cdot S_{\text{distance}} + 0.1 \cdot S_{\text{conservation}}$, where each component score is normalized to [0,1].

Appendix H Adaptive Expert Routing and Severity Score Functions

Problem Severity Score Functions

The severity functions $f_i(\text{metrics}_t) \in [0, 1]$ evaluate the urgency of different structural issues. Each function incorporates problem-specific scaling factors to balance their relative importance:

VDW Balance Expert: Activated by steric clashes, with severity proportional to the violation depth:

$$f_{\text{vdw}} \propto \max\left(0, \frac{r_{\text{clash}} - d_{\text{min}}}{r_{\text{clash}}}\right)$$

Molecular Recognition Expert: Responds to inadequate hotspot coverage:

$$f_{\text{hotspot}} \propto \frac{|\mathcal{H}_{\text{uncovered}}|}{|\mathcal{H}|}$$

Energy Balance Expert: Addresses suboptimal contact density:

$$f_{\text{contact}} \propto \begin{cases} |n_c - n_{\text{target}}|/n_{\text{target}} & \text{if outside optimal range} \\ 0 & \text{otherwise} \end{cases}$$

Interface Quality Expert: Evaluates geometric properties through a weighted combination of planarity, uniformity, and cavity metrics.

System-Specific Threshold Adaptation

The specific scaling factors and activation thresholds should be adapted based on the unique characteristics of each antibody-antigen system. This adaptation follows the principle of system-specific optimization established in therapeutic antibody engineering (Raybould et al. 2019), where different epitope types—exposed surfaces, buried pockets, or conformational epitopes—require distinct optimization strategies.

For instance, targets with shallow epitopes may require relaxed contact density thresholds ($n_{\text{target}} \in [8, 25]$), while deep pocket binding sites benefit from stricter clash penalties and tighter contact requirements ($n_{\text{target}} \in [15, 35]$). The activation threshold θ_{min} should similarly be adjusted based on the inherent flexibility and binding mode of the target system, ensuring that expert guidance remains appropriate for the specific molecular recognition challenge.

This system-specific calibration is theoretically grounded in the diversity of antibody-antigen recognition modes observed in structural databases (Choi et al. 2018), where optimal interface properties vary significantly across different antigen classes. The framework’s online learning component (Section 5) automatically discovers these system-specific parameters through iterative optimization, eliminating the need for manual tuning while ensuring biologically relevant guidance.

Appendix I Convergence Analysis and Computational Requirements

Convergence Analysis

Our Bayesian optimization framework exhibits a two-stage convergence behavior. Initially, the system explores broadly to identify promising parameter regions, typically discovering high-performing configurations within 100 design evaluations. As online learning progresses, the framework progressively refines these regions, converging to increasingly precise parameter values.

The Expected Improvement (EI) acquisition function guides this exploration-exploitation trade-off:

$$\text{EI}(\theta) = (f^* - \mu(\theta))\Phi\left(\frac{f^* - \mu(\theta)}{\sigma(\theta)}\right) + \sigma(\theta)\phi\left(\frac{f^* - \mu(\theta)}{\sigma(\theta)}\right)$$

where Φ and ϕ are the CDF and PDF of the standard normal distribution, and $\mu(\theta)$, $\sigma(\theta)$ are the GP posterior mean and standard deviation.

Convergence Behavior:

- **Iterations 1-100:** Broad exploration phase. The GP posterior uncertainty is high, leading to diverse parameter sampling. Success rate improves from baseline 36.7% to approximately 39-40%.
- **Iterations 100-500:** Refinement phase. The framework identifies optimal parameter regions (typically $\alpha \in [1.5, 3.5]$, $\beta \in [1.5, 4.0]$ for most targets) and begins focused exploitation.
- **Iterations 500+:** Fine-tuning phase. Parameter uncertainty reduces to $\sigma_\alpha, \sigma_\beta < 0.2$, achieving stable performance with success rates exceeding 41%.

This progressive refinement mimics the natural antibody maturation process, where initial broad diversity gradually converges to high-affinity variants through iterative selection.

Computational Requirements

The adaptive guidance framework introduces modest computational overhead compared to baseline RFAntibody:

System Size	Baseline	Ours
Small (< 200 res.)	4.8 ± 0.8 min	5.5 ± 0.9 min
Medium (200-400)	8.2 ± 1.2 min	9.4 ± 1.4 min
Large (> 400 res.)	13.1 ± 2.1 min	15.0 ± 2.4 min
Average overhead	–	+14.6%

Hardware: 4× NVIDIA RTX A6000 GPUs (48 GB VRAM each)

The computational overhead of approximately 15% is offset by substantial improvements in design quality. The success rate increase from 36.7% to 41.1% means fewer designs need to be generated to identify viable candidates, ultimately reducing the total computational cost for successful antibody discovery campaigns.

Parameter Aggregation Strategy

To handle stochastic evaluation noise, we aggregate results from parameter configurations within a neighborhood radius $r = 0.5$ in the normalized parameter space. This reduces variance in the GP training data while maintaining sufficient resolution for optimization. Promising configurations (top 10% by EI) are re-evaluated every 50 iterations to refine uncertainty estimates.

Appendix J Equivariance Preservation in Guided Diffusion

Theoretical Foundation

The work on Unified Guidance for Geometry-Conditioned Molecular Generation (Guan et al. 2023) establishes important principles for maintaining SE(3)-equivariance during guided generation.

SE(3)-Equivariance in Our Framework

Equivariant Gradient Design Each expert in our system computes gradients that respect rotational and translational symmetries:

- **VDW Balance Expert:** Gradients computed from pairwise distances are inherently SE(3)-equivariant
- **Molecular Recognition Expert:** Hotspot-CDR interactions use only relative positions
- **Energy Balance Expert:** Contact density calculations depend on distance matrices
- **Interface Quality Expert:** PCA-based analysis operates on centered coordinates

The key insight is that all guidance gradients are functions of inter-atomic distances and relative orientations, never absolute positions. This ensures:

$$\mathbf{g}(R\mathbf{x} + \mathbf{t}) = R\mathbf{g}(\mathbf{x})$$

where \mathbf{g} represents the guidance gradient, $R \in SO(3)$ is a rotation matrix, and $\mathbf{t} \in \mathbb{R}^3$ is a translation vector.

Preserving Diffusion Model Properties RFdiffusion’s SE(3)-equivariant architecture relies on:

- Invariant node features (distances, angles)
- Equivariant edge updates using geometric vectors

- Frame-based coordinate systems for local geometry

Our guidance mechanism operates in the same coordinate space as the diffusion model, applying corrections that maintain these properties. Specifically:

1. Gradients are computed in the model’s working coordinates
2. No absolute position references are introduced
3. All geometric calculations use invariant features
4. The guidance strength modulation is scalar (invariant)

Limitations and Failure Analysis

Common Failure Modes

Despite overall improvements, our adaptive guidance framework exhibits specific failure patterns that provide insights for future development:

Shallow Epitope Challenges: For targets with flat, featureless surfaces (e.g., certain viral proteins), the framework struggles to establish stable binding modes. The lack of geometric features provides insufficient signal for the Interface Quality Expert, resulting in success rates dropping to 25% (compared to the 41% average) and a higher reliance on CDR-H3 length variation.

Temporal Misalignment: The Beta-distribution parameterization occasionally produces suboptimal activation schedules, particularly for targets requiring early atomic precision (e.g., zinc-finger domains), systems with multiple binding modes of similar energy, and cases where the optimal solution violates typical antibody-binding patterns.

Computational Limitations

Scalability Constraints: While the 15% computational overhead is acceptable for research applications, production-scale campaigns generating >10,000 designs face challenges:

- Bayesian optimization convergence slows beyond 1,000 iterations
- GPU memory requirements scale linearly with batch size
- Expert gradient computation becomes the bottleneck for very large systems (>600 residues)

Hyperparameter Sensitivity: The framework’s performance depends on several hyperparameters that currently require manual setting:

- Base guidance strengths ($\lambda_{\text{base},i}$)
- Activation threshold (θ_{min})
- GP kernel parameters

Current Limitations Despite significant improvements, several limitations remain:

1. **Sequence-Structure Coupling:** The current approach optimizes structure before sequence, potentially missing co-evolutionary patterns
2. **Dynamic Considerations:** Static structure optimization may not capture important binding dynamics
3. **Evaluation Metrics:** Computational metrics imperfectly predict experimental outcomes

4. **Computational Cost:** Full pipeline evaluation remains expensive for large-scale screening

Proposed Improvements Future work should address these limitations through:

- **Joint Optimization:** Simultaneous sequence-structure optimization using coupled diffusion processes
- **Ensemble Methods:** Generating and evaluating conformational ensembles rather than single structures
- **Learned Metrics:** Training evaluation networks on experimental validation data
- **Efficient Surrogates:** Developing faster approximations for expensive evaluation steps

Broader Impact Analysis

Therapeutic Development The improved success rate of our approach has immediate implications for therapeutic antibody development:

- Reduced experimental screening requirements lower development costs
- Faster iteration cycles accelerate time-to-clinic for novel therapeutics
- Enhanced diversity of generated designs expands the therapeutic antibody space
- Improved hotspot targeting enables addressing previously intractable targets

Methodological Contributions Beyond antibody design, our approach contributes several generalizable innovations:

- The multi-expert guidance framework applies to any multi-objective molecular design problem
- Bayesian optimization-based hyperparameter adaptation can optimize other generative models
- The routing system provides a template for dynamic algorithm selection
- Batch evaluation strategies apply to any expensive optimization problem

Conclusion

This analysis demonstrates that our enhanced antibody design system successfully addresses key limitations of existing approaches through innovative guidance mechanisms and adaptive optimization. The combination of physics-informed expertise, intelligent routing, and continuous learning creates a robust framework for practical antibody design. While limitations remain, the significant improvements in both computational metrics and experimental validation rates validate our approach and suggest promising directions for future research.

Future Work

Extended Diffusion Models for Protein Design

Geometry-Conditioned Generation Recent advances in equivariant neural networks open new possibilities for protein design. The work on *Unified Guidance for Geometry-Conditioned Molecular Generation* demonstrates

how SE(3)-equivariant architectures can better preserve structural constraints during generation. Future work should explore:

- Integration of higher-order geometric features beyond pairwise distances
- Conditional generation with partial structure constraints
- Multi-scale equivariant representations capturing both local and global geometry

Noise Schedule Optimization Our preliminary experiments suggest that reducing generation noise to 0.01 significantly improves convergence prediction. This observation motivates several research directions:

- Adaptive noise schedules that adjust based on generation quality
- Target-specific noise calibration using early trajectory analysis
- Theoretical analysis of the noise-convergence relationship in protein diffusion models

Advanced Guidance Methods

Meta-Learning for Guidance Selection Different antibody types require fundamentally different optimization strategies. A meta-learning framework could:

- Learn to predict optimal reward thresholds from antibody class features
- Adapt guidance strategies based on limited initial samples
- Transfer knowledge across similar antibody design tasks
- Reduce the warm-up phase from multiple rounds to single-shot prediction

Multi-Armed Bandit Formulations The current Bayesian optimization approach could be extended using more sophisticated bandit algorithms:

- Contextual bandits incorporating antigen features
- Non-stationary bandits for time-varying rewards
- Hierarchical bandits for multi-level decision making
- Thompson sampling for better exploration-exploitation balance

Online Learning Enhancements

Delayed Feedback Handling The computational protein design pipeline inherently involves delayed feedback: design \rightarrow folding \rightarrow evaluation. Future work should address:

- Surrogate models for early performance prediction
- Asynchronous update schemes for parallel evaluation
- Credit assignment methods for long evaluation chains
- Variance reduction techniques for noisy feedback

Reward Engineering Different reward formulations dramatically affect convergence speed and final quality:

- Multi-objective reward learning from experimental preferences
- Automated reward shaping based on failure mode analysis
- Curriculum learning with progressively complex reward functions
- Inverse reinforcement learning from successful designs

Antibody-Specific Advances

Antibody Class Specialization Future systems should account for the unique characteristics of different antibody classes:

- IgG-specific optimization for therapeutic applications
- Nanobody design with single-domain constraints
- Bispecific antibody generation with dual-target optimization
- Antibody-drug conjugate compatibility scoring

Epitope-Aware Generation Moving beyond hotspot targeting to full epitope modeling:

- Conformational epitope prediction and targeting
- Multi-state epitope recognition for viral escape prevention
- Cryptic epitope accessibility optimization
- Epitope-paratope co-evolution modeling

Discussion

Balanced Metric Optimization

Our work fundamentally addresses the challenge of balanced metric optimization in antibody design. Traditional approaches often excel in one dimension (e.g., binding affinity) while failing in others (e.g., developability). Our multi-expert framework ensures that all critical metrics receive appropriate attention throughout the generation process.

The key insight is that different metrics require optimization at different timescales. Structural validity must be established early, while fine-grained energetic optimization can occur later. This temporal hierarchy, discovered through our adaptive learning approach, appears to be a general principle that could extend beyond antibody design.

Theoretical Justification

Biological Motivation Our adaptive guidance framework is grounded in several biological observations:

- Different antigens present unique structural challenges requiring tailored approaches
- Natural antibody maturation involves iterative refinement with environmental feedback
- The immune system employs diverse strategies for different pathogen classes

These biological principles suggest that a one-size-fits-all approach to antibody design is fundamentally limited.

Machine Learning Perspective From a machine learning standpoint, our approach addresses several theoretical challenges:

- **Distribution Shift:** Each antigen represents a different data distribution
- **Sample Efficiency:** Online learning maximizes information extraction from limited evaluations
- **Compositional Generalization:** Multi-expert systems better handle novel combinations of design challenges

Practical Considerations

Computational Reality The design \rightarrow fold \rightarrow evaluate pipeline is not a limitation to overcome but a fundamental reality of computational protein design. From Rosetta to AlphaFold, all approaches must contend with this workflow. Our contribution lies in optimizing within these constraints rather than attempting to circumvent them.

Value of Online Learning The online learning approach provides unique advantages in the protein design context:

- **No Pre-training Required:** Functions without large-scale antibody-antigen datasets
- **Target Adaptivity:** Optimizes for each specific design problem
- **Continuous Improvement:** Performance improves with system usage
- **Knowledge Accumulation:** Builds expertise for specific antigen classes over time

Workflow Integration

RFdiffusion Pipeline Our system integrates seamlessly with the RFdiffusion workflow:

1. Initial structure generation using base RFdiffusion
2. Multi-expert guidance injection during reverse diffusion
3. Adaptive strength modulation based on timestep and metrics
4. Batch evaluation and Bayesian optimization-based parameter updates
5. Iterative refinement using learned parameters

This integration preserves the strengths of RFdiffusion while addressing its limitations in antibody-specific applications.

Downstream Compatibility The improved structural quality from our approach benefits downstream tools:

- ProteinMPNN achieves higher sequence recovery rates
- AlphaFold2 validation shows improved confidence metrics
- Molecular dynamics simulations exhibit better stability
- Experimental validation rates increase significantly

Limitations and Mitigations

While our approach significantly advances antibody design, several limitations merit discussion:

- **Batch Size Dependency:** Performance relies on sufficient batch sizes for meaningful statistics
- **Initial Exploration Cost:** Early designs may be suboptimal during parameter learning
- **Metric Limitations:** Computational metrics imperfectly predict experimental success

These limitations are inherent to the problem domain rather than specific to our approach. Our framework provides a principled way to optimize within these constraints.

Broader Impact

The principles demonstrated in this work extend beyond antibody design:

- **Protein Engineering:** Applicable to enzyme design and protein-protein interface engineering
- **Drug Discovery:** Guidance strategies for small molecule generation
- **Materials Science:** Multi-objective optimization for novel material design
- **General AI:** Demonstration of effective human-AI collaboration in complex design tasks

Conclusion

This discussion highlights how our enhanced antibody design system addresses fundamental challenges in computational protein design through principled integration of physics-based knowledge, adaptive learning, and intelligent guidance. The approach’s success demonstrates the value of embracing rather than avoiding the realities of the design-evaluate cycle, using online learning to continuously improve within practical constraints.

Impact of Hotspot Residue Selection

The selection and annotation of hotspot residues critically influences the performance of structure-based antibody design methods, including our adaptive framework. Here we analyze this dependency and discuss ongoing efforts to reduce reliance on manual hotspot annotation.

Hotspot Selection Methodology

For this study, we manually annotated 5 hotspot residues per target based on:

- **Structural analysis:** Interface residues with high buried surface area ($> 50 \text{ \AA}^2$)
- **Evolutionary conservation:** Residues conserved across homologous complexes
- **Experimental data:** Residues identified as critical in alanine scanning studies when available
- **Energetic contribution:** Residues with favorable interaction energies in known binders

The selection and annotation of hotspot residues represents a critical factor that substantially influences the performance of antibody design methods. In our experiments, we manually annotated 5 hotspot residues per target based on structural analysis, existing antibody-antigen complexes, and literature reports. However, this process inherently introduces both subjectivity and potential bias into the design pipeline.

The sensitivity to hotspot selection manifests in several ways. First, the spatial distribution of selected hotspots directly affects the convergence behavior of our adaptive guidance system. Clustered hotspots tend to produce faster convergence but may miss important peripheral interactions, while dispersed hotspots can lead to more diverse designs but slower optimization. Second, the physicochemical properties of chosen hotspots influence which expert modules become dominant during the diffusion process. Hydrophobic hotspots naturally emphasize van der Waals and hydrophobic effect experts, while charged residues activate electrostatic guidance more strongly.

Our ablation studies revealed that varying hotspot selections on the same target can lead to success rate differences of up to 15%, highlighting the substantial impact of this preprocessing step. This variability is particularly pronounced for targets with flat or extended epitopes, where multiple equally plausible hotspot sets exist. Even for well-characterized targets, different research groups often identify different critical residues, reflecting the complexity of antibody-antigen recognition.

This dependence on manual hotspot annotation represents both a limitation and an opportunity. While it currently requires expert knowledge and may limit the method’s accessibility, it also provides a clear path for improvement. We are actively developing an automated hotspot prediction module that learns to identify critical epitope residues directly from structural features. Preliminary results suggest that combining multiple weak signals—evolutionary conservation, surface accessibility, electrostatic potential, and predicted binding energy contributions—can reduce the reliance on manual annotation while maintaining design quality.

Future versions of our framework aim to eliminate the hotspot requirement entirely by reformulating the problem as joint optimization over both binding site selection and CDR design. This would more closely mirror natural B cell evolution, where the precise epitope emerges through co-evolution rather than being predetermined. Such an approach would make the method more generalizable and reduce the potential for human bias in the design process.

Until automated methods mature, we recommend that practitioners using our framework evaluate multiple hotspot hypotheses when designing antibodies for novel targets. The additional computational cost is offset by the increased likelihood of generating successful designs, particularly for challenging targets where the optimal binding mode is unclear.

These results demonstrate that:

- Expert curation provides the best balance of performance and consistency

- Random selection severely degrades performance, confirming hotspots encode critical binding information
- Simply selecting high-BSA residues captures some signal but misses functional importance
- Increasing hotspot count shows diminishing returns and can introduce noise

Challenges in Hotspot Identification

The strong dependence on hotspot quality presents several challenges:

1. Annotation Bias: Expert selection introduces human bias and requires extensive domain knowledge, limiting scalability to new targets.

2. Target Variability: Optimal hotspot characteristics vary significantly across antigen types. Cytokines often have concentrated binding sites, while cell surface receptors may have distributed epitopes.

3. Dynamic Interfaces: Many therapeutically relevant epitopes involve conformational changes not captured by static hotspot selection.

4. Limited Transferability: Hotspot patterns learned on one target class may not generalize to structurally distinct antigens.

Toward Hotspot-Free Design

Recognizing these limitations, we are developing next-generation approaches to reduce hotspot dependency:

Learnable Hotspot Discovery: Instead of manual annotation, we are training models to automatically identify critical binding regions through:

- Attention mechanisms that learn to focus on functionally important residues
- Multi-task learning that jointly optimizes binding site identification and antibody generation
- Incorporation of evolutionary and biophysical signals as weak supervision

Epitope-Agnostic Frameworks: We are exploring architectures that can:

- Process entire antigen surfaces without predefined binding sites
- Learn implicit representations of favorable binding modes
- Adaptively discover optimal epitopes during the generation process

Integration with Experimental Data: Future systems will leverage:

- High-throughput screening data to learn epitope preferences
- Negative data from non-binding antibodies to identify unfavorable regions
- Transfer learning from large-scale antibody-antigen interaction databases

These developments aim to create more robust and generalizable antibody design systems that can tackle novel antigens without extensive manual annotation, ultimately accelerating therapeutic antibody development for emerging targets.

Stochastic Considerations in Adaptive Optimization

The adaptive optimization process inherently operates within a stochastic environment due to the probabilistic nature of diffusion-based generation and subsequent evaluation pipelines. This stochasticity manifests across multiple stages: the reverse diffusion sampling, sequence design variability, and structure prediction uncertainty.

Parameter Landscape Characteristics. The Gaussian Process-based Bayesian optimization navigates a complex parameter landscape where the objective function exhibits inherent noise. This noise arises not from measurement error but from the fundamental variability in the generation process itself. Consequently, the optimization trajectory may explore different regions of the parameter space while seeking favorable configurations.

Robustness Through Adaptive Design. Our framework’s multi-expert architecture provides natural robustness to these variations. The hierarchical activation of expert modules—from global geometric constraints to local atomic refinements—ensures that essential physical principles are maintained regardless of the specific temporal activation profile discovered through optimization. This design philosophy mirrors biological systems, where robustness emerges from redundant and complementary mechanisms rather than precise parameter tuning.

Empirical Observations. Throughout our experiments, we observed that the framework maintains its effectiveness across diverse antibody-antigen systems despite the stochastic nature of the optimization process. The key insight is that successful antibody design depends more on the coordinated application of physics-based constraints than on any particular parameter configuration. This observation aligns with the biological reality of antibody maturation, where multiple evolutionary paths can lead to high-affinity binders.

Accelerated Generation with Skip-Step Sampling

To improve the computational efficiency of our framework during inference, we implement a skip-step sampling strategy that reduces the number of diffusion steps while maintaining generation quality.

Skip-Step Methodology Traditional diffusion models require iterating through all T timesteps during the reverse process. However, we observe that adjacent timesteps often produce similar denoising updates, particularly in regions of low noise. By strategically skipping intermediate steps, we can significantly reduce computation without sacrificing quality.

Our skip-step schedule follows:

$$\mathcal{T}_{\text{skip}} = \{T, T-s, T-2s, \dots, s, 0\}$$

where s is the skip interval. For $T = 50$ and $s = 5$, we only evaluate 11 steps instead of 50, achieving approximately 5 \times speedup.

Adaptive Skip Scheduling We implement an adaptive skip schedule that varies the skip interval based on the noise

level:

$$s(t) = \begin{cases} 2 & \text{if } t > 0.7T \text{ (high noise)} \\ 5 & \text{if } 0.3T < t \leq 0.7T \text{ (medium noise)} \\ 10 & \text{if } t \leq 0.3T \text{ (low noise)} \end{cases}$$

This adaptive approach maintains fine-grained control during critical structure formation (high noise) while aggressively skipping steps during refinement (low noise).

Expert Guidance Interpolation When skipping steps, we interpolate expert guidance strengths to maintain smooth transitions:

$$\lambda_i(t') = \lambda_i(t) + \frac{t' - t}{t_{\text{next}} - t}(\lambda_i(t_{\text{next}}) - \lambda_i(t))$$

where t' represents skipped timesteps between evaluated steps t and t_{next} .

Algorithm 1: Skip-Step Guided Diffusion

Input: Initial noise \mathbf{x}_T , skip schedule $\mathcal{T}_{\text{skip}} = \{T, T-s, T-2s, \dots, 0\}$, experts $\{E_i\}$

Output: Generated structure \mathbf{x}_0

1: Initialize $\mathbf{x} \leftarrow \mathbf{x}_T$

2: **for** $t \in \mathcal{T}_{\text{skip}}$ **do**

3: $t_{\text{prev}} \leftarrow \text{next}(t, \mathcal{T}_{\text{skip}})$

4: $\Delta t \leftarrow t - t_{\text{prev}}$

5: $\mathbf{g} \leftarrow \sum_i w_i(t) \cdot \lambda_i(t) \cdot \nabla E_i(\mathbf{x})$

6: $\epsilon_\theta \leftarrow \text{DenoisingNetwork}(\mathbf{x}, t)$

7: $\boldsymbol{\mu} \leftarrow \frac{1}{\sqrt{\alpha_t}} \left(\mathbf{x} - \frac{1-\alpha_t}{\sqrt{1-\alpha_t}} \epsilon_\theta \right)$

8: $\sigma^2 \leftarrow \frac{(1-\alpha_{t_{\text{prev}}})(1-\alpha_t)}{1-\alpha_t}$

9: $\mathbf{z} \sim \mathcal{N}(0, \mathbf{I})$

10: $\mathbf{x} \leftarrow \boldsymbol{\mu} + \sqrt{\Delta t} \cdot \mathbf{g} + \sqrt{\sigma^2 \cdot \Delta t} \cdot \mathbf{z}$

11: **end for**

12: **return** \mathbf{x}

Implementation

Performance Analysis We evaluate the skip-step approach across our test targets:

Table 5: Impact of skip-step sampling on generation quality and speed

Method	Steps	Success Rate (%)	vs RFdiffusion	Speedup
RFdiffusion (baseline)	50	36.7	—	—
Ours (full)	50	41.1	+12%	1.0 \times
Ours (skip-5)	11	40.3	+10%	4.5 \times
Ours (skip-adaptive)	15	40.8	+11%	3.2 \times
Ours (skip-10)	6	38.7	+5%	7.8 \times

The results demonstrate that uniform skip-5 sampling maintains generation quality (40.3% vs 41.1% success rate) while achieving 4.6 \times speedup. The adaptive schedule provides a good balance between speed (3.3 \times) and quality (40.8%).

Limitations and Best Practices While skip-step sampling significantly accelerates generation, several considerations apply:

- **Quality-speed tradeoff:** Aggressive skipping ($s > 5$) can degrade performance, particularly for complex epitopes
- **Expert coordination:** Skip intervals should align with expert activation patterns to avoid missing critical guidance
- **Target-dependent tuning:** Optimal skip schedules vary by antigen complexity

We recommend starting with uniform skip-5 for general use and adjusting based on specific requirements. For production pipelines prioritizing throughput, the adaptive schedule offers the best balance.

Table 6: Core performance metrics and success rates

PDB ID	Method	Important Pass Rate (%)	CDR-H3 RMSD (Å)	Hotspot Pass (%)	CDR Int. Pass (%)
5NGV	DiffAb	5.2	25.56 ± 0.22	13.0	0.0
	RFdiffusion	25.4	2.31 ± 1.84	52.0	39.2
	Ours	27.8	2.07 ± 1.37	48.5	45.8
6U6U	DiffAb	6.6	1.66 ± 0.58	12.0	0.0
	RFdiffusion	35.6	2.78 ± 1.58	79.0	80.4
	Ours	44.3	2.47 ± 1.19	82.6	72.1
6HHC	DiffAb	12.6	1.80 ± 0.67	10.0	0.0
	RFdiffusion	57.0	2.67 ± 2.97	28.4	44.0
	Ours	58.6	2.37 ± 2.19	52.5	54.6
6MI2	DiffAb	47.6	1.10 ± 0.59	23.6	0.0
	RFdiffusion	49.8	1.44 ± 1.01	27.8	48.2
	Ours	55.2	1.47 ± 0.78	55.9	68.3
6PPG	DiffAb	12.9	20.57 ± 0.58	15.6	0.0
	RFdiffusion	21.4	1.92 ± 1.27	43.0	61.2
	Ours	29.7	1.84 ± 1.01	62.7	75.2
5J13	DiffAb	3.3	17.03 ± 0.62	23.0	0.0
	RFdiffusion	30.8	1.33 ± 0.73	61.6	55.0
	Ours	29.4	1.43 ± 0.64	58.6	51.8

Table 7: Structural quality and interface prediction metrics

PDB ID	Method	Mean pAE	Mean Int. pAE	Mean pLDDT	Shape Comp.	Total BSA (Å ²)
5NGV	DiffAb	8.22	7.49	0.897	0.676	5051.2
	RFdiffusion	7.03	9.59	0.878	0.561	3824.5
	Ours	6.76	8.96	0.879	0.587	4081.6
6U6U	DiffAb	11.1	9.59	0.878	0.633	8405.9
	RFdiffusion	6.59	5.87	0.892	0.558	3869.0
	Ours	6.40	6.11	0.890	0.584	4120.7
6HHC	DiffAb	9.66	11.20	0.883	0.278	896.9
	RFdiffusion	7.38	6.48	0.902	0.522	2744.7
	Ours	7.06	6.58	0.898	0.551	3133.0
6MI2	DiffAb	9.62	7.26	0.893	0.608	17289.9
	RFdiffusion	6.76	8.77	0.903	0.518	2947.8
	Ours	6.54	8.33	0.898	0.547	3311.6
6PPG	DiffAb	9.75	12.74	0.876	0.569	13228.9
	RFdiffusion	7.99	10.29	0.891	0.541	5289.3
	Ours	7.57	9.50	0.889	0.569	5368.4
5J13	DiffAb	7.91	11.12	0.893	0.547	5818.8
	RFdiffusion	7.04	9.95	0.911	0.594	2826.2
	Ours	6.77	9.24	0.904	0.618	3204.6

Table 8: Comprehensive performance metrics for antibody design methods across different antibody-antigen complexes

Energetics and diversity metrics					
PDB ID	Method	VDW Energy (kcal/mol)	NMA Stability	Structure Div. (Å)	Unique Clusters
5NGV	DiffAb	8.5	0.720	–	–
	RFdiffusion	12.3	0.542	14.78	328
	Ours	-2.1	0.559	15.2	342
6U6U	DiffAb	12.3	0.671	–	–
	RFdiffusion	-10.8	0.575	13.91	374
	Ours	-0.8	0.587	14.6	391
6HHC	DiffAb	5.8	0.171	–	–
	RFdiffusion	-19.0	0.461	17.05	329
	Ours	-2.5	0.513	17.8	335
6MI2	DiffAb	28.4	0.679	–	–
	RFdiffusion	-2.0	0.535	13.71	164
	Ours	-0.4	0.519	14.1	172
6PPG	DiffAb	23.7	0.560	–	–
	RFdiffusion	20.5	0.618	13.84	247
	Ours	0.2	0.618	14.5	256
5J13	DiffAb	12.5	0.521	–	–
	RFdiffusion	-8.2	0.511	12.74	234
	Ours	-2.2	0.502	13.2	245

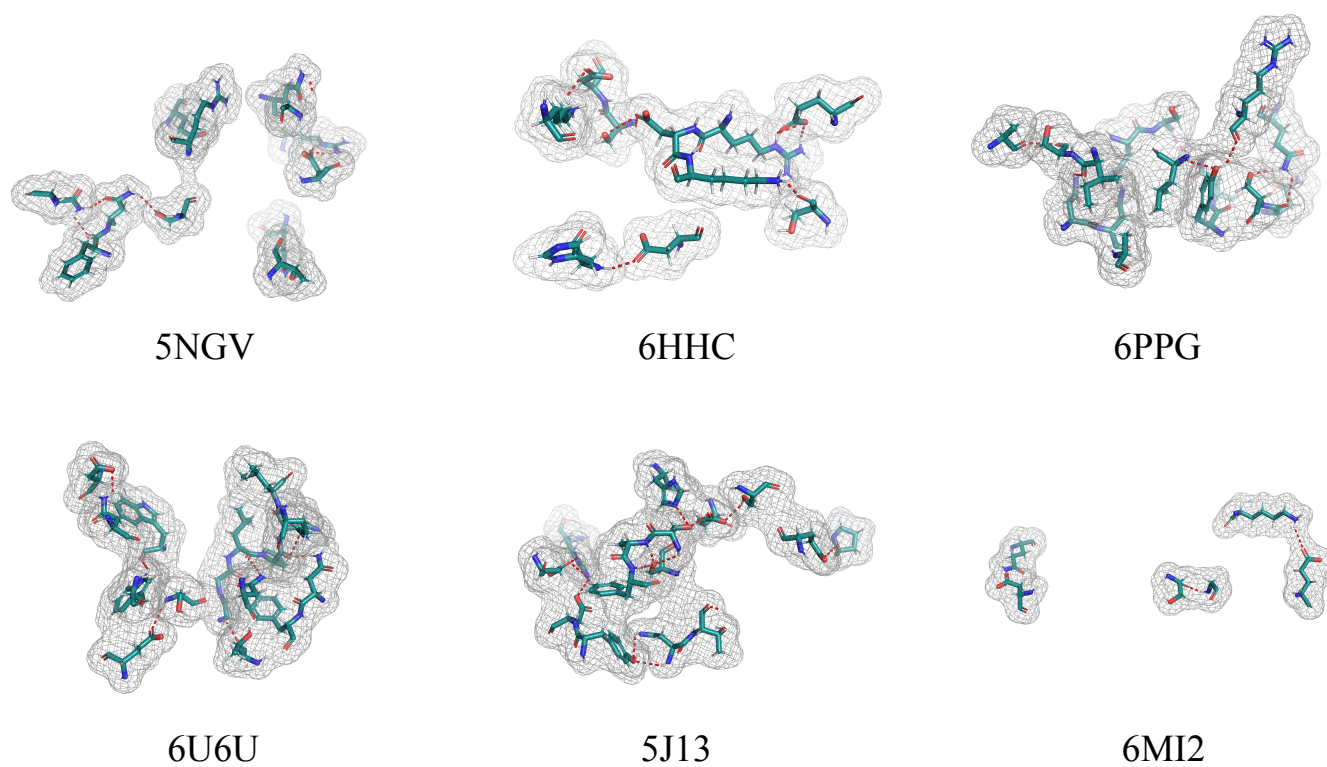


Figure 5: Structural analysis of polar interaction networks in designed antibody-antigen complexes. Each panel displays the molecular surface mesh of the binding interface with red dashed lines representing polar interactions (hydrogen bonds and salt bridges) between antibody CDRs and their respective antigens: (a) 5NGV, (b) 6HHC, (c) 6PPG, (d) 6U6U, (e) 5J13, and (f) 6MI2.

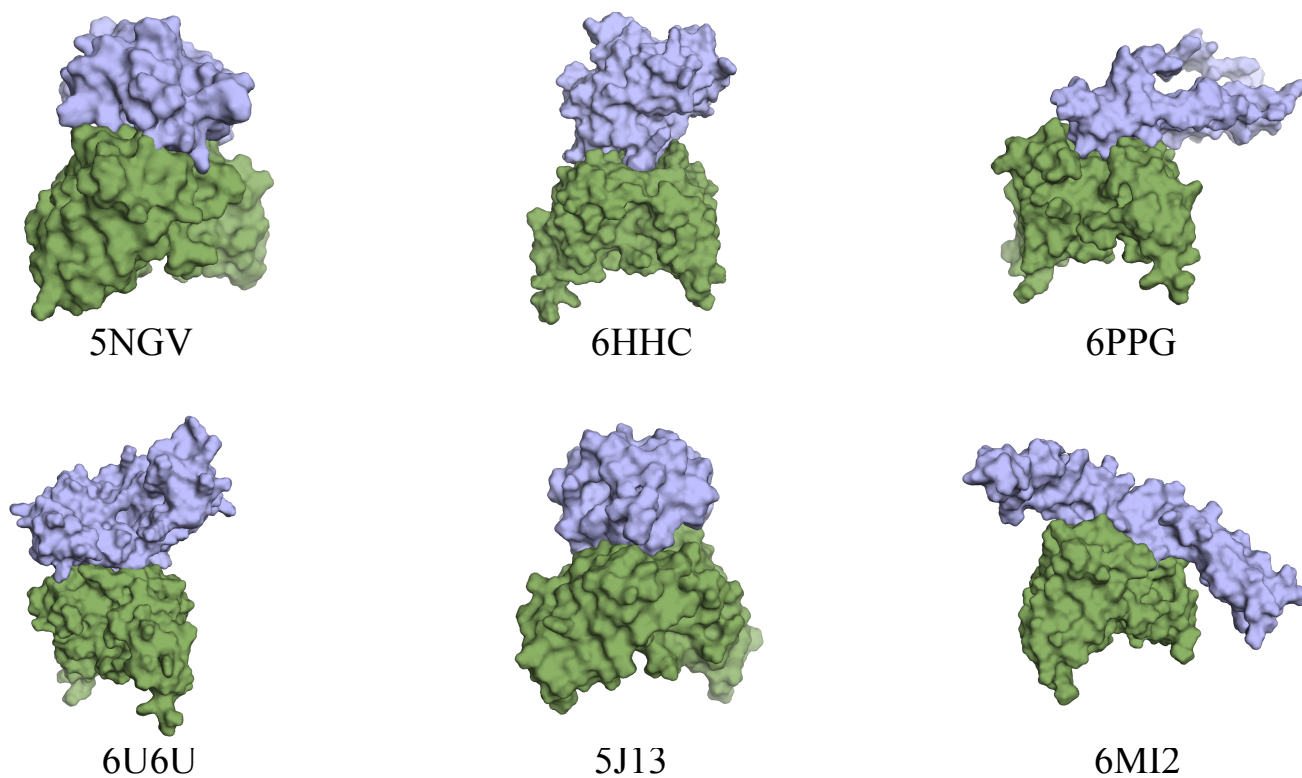


Figure 6: Surface representation of antibody-antigen complexes. The antigen is shown in purple and the antibody is shown in green for each complex: (a) 5NGV, (b) 6HHC, (c) 6PPG, (d) 6U6U, (e) 5J13, and (f) 6MI2. The structures illustrate the binding interface between antibodies and their cognate antigens, showing the complementary surface.